Table of Contents

List of Abbreviations

Geometric parameters

ϕ	Stagger angle	°
c	Chord (distance between leading edge and trailing edge)	m
c_x	Axial chord, as c projected onto shaft axis	m
D_m	Mean diameter of blade	m
h	Height (blade height between hub and tip)	m
h/c	Blade aspect ratio	-
h/c_x	Axial blade aspect ratio	-
o_t	Throat opening	m
R	Total radius of rotor (axis to tip)	m
R_h	Radius of hub	m
R_m	Mean radius of blade	m
R_t	Radius of tip	m
R_{ht}	Hub-to-tip radius ratio	-
s	Pitch or spacing (distance between two adjacent blades)	m
t	Blade thickness	m
t_{et}	Trailing edge thickness	m
t_{max}	Maximum blade thickness	m

Loss model variabes

$\Delta\phi^2$	Energy loss coefficient for trailing edge losses	-
f_{Re}	Reynolds number correction for profile loss	-
f_{AR}	Aspect ratio correction for secondary loss	-

K_1	Correction term for exit Mach number	-
K_2	Correction term for channel acceleration	-
K_S, K_3	Corrections for subsonic Mach number in secondary losses	-
K_P	Correction term for high Mach numbers	-
K_P, K_1, K_2	Correction terms for loss models	-
Y	Pressure loss coefficient referred to dynamic exit pressure	-
Y_P	Profile loss coefficient	-
Y_S	Secondary loss coefficient	-
Y_{shock}	Profile shock loss coefficient	-
Y_{TC}	Tip clearance loss coefficient	-
Y_{TET}	Trailing edge loss coefficient	-

Subindices and stages

0	Total variable (static + dynamic)
1	Start of turbine stage, entry to vane/stator
2	Stator exit, entry to rotor
3	Rotor exit, end of turbine stage
s	Isentropic value

Thermodynamic variables

ΔH	Enthalpy change	$\mathrm{J\,kg^{-1}}$
η	Isentropic efficiency	-
γ	Heat capacity ratio	
ψ	Stage loading	-
ρ	Static density	$\mathrm{kg\,m^{-3}}$
ρ_0	Total density	$\mathrm{kg\,m^{-3}}$
φ	Flow coefficient or flow function	-
C_p	Heat capacity	
GR	Degree of reaction	-

P	Static pressure	Pa
P_0	Total pressure	Pa
q	Dynamic pressure	Pa
R	Specific gas constant	$\mathrm{J\,kg^{-1}\,K^{-1}}$
T	Static temperature	K
T_0	Total temperature	K
T_s	Ideal static temperature	K

Flow velocities and angles

α_1	Entry angle in vane (between v_1 and shaft axis)	rad
α_2	Exit angle in vane (between v_2 and shaft axis)	rad
α_m	Mean gas angle	rad
β_2	Entry angle in rotor (between w_2 and shaft axis)	rad
β_3	Exit angle in rotor (between w_3 and shaft axis)	rad
Ω	Angular velocity	$\mathrm{rad\,s^{-1}}$
a	Speed of sound	$\mathrm{m\,s^{-1}}$
M	Mach number	
RPM	Revolutions per minute	$\mathrm{rev\,min^{-1}}$
u	Peripheral velocity	$\mathrm{m\,s^{-1}}$
v_u	Tangential component of velocity in fixed axes	$\mathrm{m\,s^{-1}}$
v_x	Axial component of velocity in fixed axes	$\mathrm{m\,s^{-1}}$
w_u	Tangential component of velocity in fixed axes	$\mathrm{m\,s^{-1}}$
w_x	Axial component of velocity in rotating axes	$\mathrm{m\,s^{-1}}$

Chapter 1

Introduction

1.1 Project aims and overview

Turbines represent some of the oldest and most versatile sources of power. Most of the electricity generated this year [1], and essentially all airborne commercial transport, is based on a turbine's fundamental principle: rotating machine which extracts kinetic energy from a fluid flow.

For over 80 years [2], airplanes have been propelled by gas turbines, in which turbines evidently play a fundamental role. Over a period nearly as extensive, loss correlations and models have been proposed, tested, discarded, readjusted, and all in search of tools which can predict the behavior seen in this component.

The aim of this project is the creation of **a simulation and prediction tool for high-pressure axial turbines, including the most relevant loss phenomena present in expansive turbine machinery**. The final result is a software tool which allows the user to define the required work and geometric constraints, and which provides in turn a turbine model which minimizes energy losses for the desired performance, with a strong predictive power.

The tool consists of a 1-dimensional mean-line calculation tool for a single stage or first stage of a high-pressure turbine, to be used in the preliminary phases of a turbine design. With only the most basic constraints and requirements, the user is able to determine the basic functional parameters of the turbine, as well as the efficiencies of each component, and the general geometrical definition of the rotor blades. In order to calculate the aerodynamic losses and subsequent drop in efficiency, a series of loss correlation models are reviewed, discussed, and implemented. Additionally, a quick overview of relevant parameters and limits is made, so as to increase the predictive power of the tool and its design accuracy.

1.1.1 State of the art

This project was selected to fill a gap regarding the application of loss models to the turbine design process. Many turbine design programs exist which apply 3-dimensional models to the aerodynamic flow field, and can predict with a high accuracy the real performance of a turbine stage. The detailed design of a blade profile is achieved through CFD software, sometimes including machine-learning, generic algorithms, or other advanced–but computationally

expensive–tools [3–5].

Thus, a more straightforward tool also has its applications. The relatively simple 1-dimensional tool can be used to select a general configuration from among all the available variables, since running it is both quick and easy to automate for a variety of possible entry cases. The program, once run on a given problem, provides the necessary geometric variables to be used as the inputs to more complex design programs. This simplifies the design process, and reduces the number of analyses made on the more expensive and more time-consuming programs.

As for the implementation itself, a number of steps in the turbine design process which were historically completed by hand have here been adapted for use with open-source optimization functions, which is a novel inclusion in this sector. On the other hand, rather than apply the loss models to a particular case of turbine, this tool aims to calculate the optimal solution for any given problem, allowing the user to define the requirements, desired constraints and assumptions. The program completes a theoretical solution and subsequently applies the loss models to calculate the optimal solution with highest efficiency for the given case.

The tool presented here should never be confused with a complex turbine design tool. Two-dimensional models, which calculate along the blade leading edge rather than use a mean-line simplification, provide much more accurate estimates of aerodynamic loss. Other models include loss phenomena which have not been included here, or use more precise equations for calculations between analysis points.

For an initial analysis, however, the proposed solution provides relatively accurate results (see **??** for a discussion of the results obtained from test cases). Additionally, the simplicity of use, and versatility for a wide range of designs, means the tool could be useful for narrowing down the parameters for the desired solution.

1.1.2 Loss models

The key element in the design tool optimization is the inclusion of loss correlations which enable the modeling of several distinct aerodynamic loss phenomena in the turbine. This inclusion drastically increases the predictive power of the design tool for turbine performance, bringing the simulated result closer to the real performance.

Over the last 70 years, a variety of correlations have been proposed to analyze the losses in turbines, often with drastically different results. Although computational solutions have improved significantly in recent years, the applied loss models have not changed significantly from the initial implementations made so long ago. For example [6], the models applied today in software dedicated to mean-line turbine estimations still uses correlations proposed by Ainley and Mathieson in their 1951 model [7].

In this paper, several empirical models will be discussed and implemented in the design tool to calculate the aerodynamic losses. This inclusion boosts the accuracy of the design tool, identifying the efficiency values through tried and tested correlations.

1.2 Objectives

This document contains the background, method, and results of the project completed as the author's *Trabajo Fin de Grado* (final project for undergraduate degree) in Aerospace Engineering. Therefore, the objectives defined for this project fall in two categories: those which increase the author's competence as the final project in an undergraduate degree, and those specific to the project's aims.

The design tool is based on a battery of reference works and existing models, as well as programming resources. The study of thermodynamic theory and loss models, as well as and the technical implementation of the design tool, provided challenges in the design process, thus increasing the author's grasp of applied methods and theory. This has been defined in the following objectives:

1. To increase the author's grasp of applied thermodynamics, turbine design models, and experimental loss correlations
2. To develop skills and experience in research and applied models in aerospace engineering disciplines, including documentation and reports
3. To learn the implementation of models and optimization methods in a high-level programming language

Finally, for the internal objectives of the project, the following list was defined:

5. To research and summarize the state-of-the-art in turbine design tools and resources
6. To research and summarize the most relevant loss phenomena models present in expansive turbine machinery
7. To develop a 1-dimensional mean-line turbine model calculation tool for any given set of requirements and constraints
8. To integrate the selected loss models and complete the optimization
9. To verify the resulting implementation with a variety of different design cases

1.3 Report disposition

This report contains the entire theoretical framework of the design tool program, as well as the description of the implementation and software, and an analysis of the results of the project.

Chapter 2 includes a quick introduction to turbo-machinery and work extraction in typical gas turbines, as well as the application of isentropic equations to solve the 1-dimensional model. Additionally, a review is made of sources of enthalpy loss, and several models which have been applied in the design tool are presented. Additionally, a quick overview of the software resources used in the implementation is made.

Chapter 3 contains the description of the initial implementation of a turbine model: all the equations and functions used in the design program are described here, and the inputs and outputs described and represented.

Chapter 4 describes the integration of the loss models described previously with the turbine design tool, including the determination of the necessary additional parameters, and the global optimization function applied to this problem.

*** complete this ***

Chapter 2

Methodology

2.1 Overview

The purpose of this project is to create a design tool which will assist in the initial preliminary design of a high-pressure axial-flow turbine given the inlet and outlet conditions, work requirements, and geometrical constraints. Although complex software exists for assistance in more complex turbine designs, their use is more complex and requires a series of input parameters, such as the details of the blade's geometry, which have not been fixed at the initial design stage. Thus, this tool provides a quick estimation of all the thermodynamic parameters in a turbine for a given problem, including the most relevant loss phenomena from experimental models. This tool will, ultimately, allow the user to determine whether or not a design is viable, as well as provide a viable estimate the turbine's efficiency.

2.1.1 Turbine geometry, nomenclature, and conventions

Before the thermodynamics of turbine expansion are detailed, a brief overview of the nomenclature used in this report is important. The reference books and documents use varying numbering for each point in a stage, depending on whether the entire engine is included in the design or not. Some authors begin their numbering at 0, whereas others begin at 1. In this section, a brief overview is made of the conventions used for **stage numbering** and **velocity triangles** is made.

The analysis in a 1-dimensional single-stage turbine model is reduced to three points (or precisely, planes) along the axial direction of the turbine: **inlet (1)**, **middle** or **stator (2)**, and **outlet** or **rotor (3)** (see fig. 2.1).

In this way, the static temperature between the rotor and stator, for example, would be written T_2, whereas the stage outlet temperature is T_3, and the inlet temperature is T_4–a value which is usually labeled T_{04} or T_{4t} if the entire engine is under analysis. Note that the number 0 is reserved to indicate the total variables, such as the sum of the dynamic and static pressures.

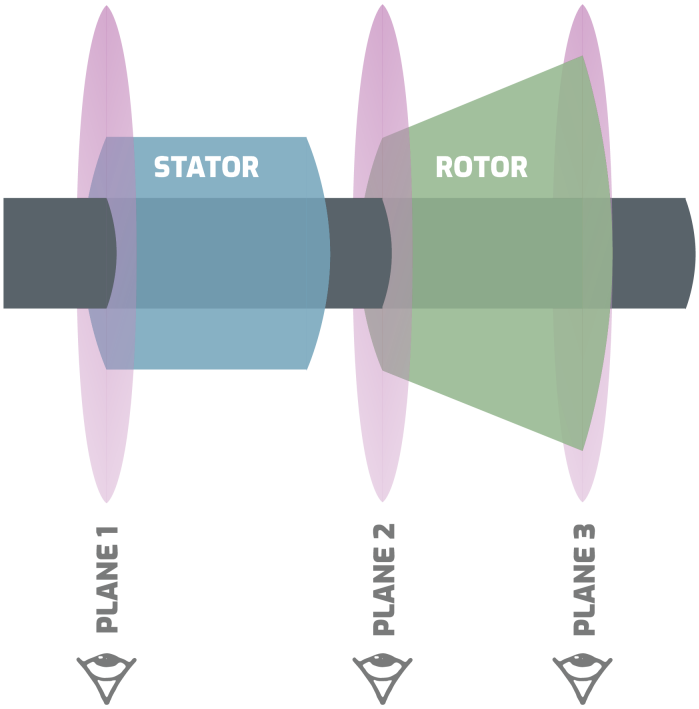

Figure 2.1: Representation of the three analysis planes on a turbine stage

Velocity triangles

The flow through the turbine in this model is measured in a two-dimensional plane–consider a cross section of a turbine stage. Therefore the velocity of the flow can be measured according to the fixed axes (where the axial direction follows the engine's shaft, and perpendicular to this is the tangential direction), and this velocity is the absolute velocity v.

On the other hand, in the rotor, the blades are moving with an angular velocity of Ω. The velocity in the reference frame of the rotating blades is the relative velocity w. These velocities are easily converted using the blade velocity $u = \Omega R$, where R is the radius of the blade section under analysis–or the mean radius $\vec{R}_m$, in this case, under the mean-line model. u, therefore, represents the peripheral speed of the mean-line (or pitchline) of the rotor.

$$\vec{v} = \vec{w} + \vec{u} = \vec{w} + \vec{\Omega} \times \vec{R}_m \tag{2.1}$$

On the other hand, each of the velocities can be projected along the shaft axis (v_x) or perpendicular to this (v_u). In the same way, the relative velocities in the rotor can also be projected: w_x, w_u. This allows for the definition of the angles.

At the inlet point (1), the flow has a velocity of $\vec{v}_1$ and an angle α_1 when entering the turbine vanes. If the flow is purely axial, then $\alpha_1 = 0$. Since the stator is by definition fixed to the engine, the rotational velocity and blade velocity are 0. (All angles are measured in terms of the engine's rotational axis.)

Exiting the stator, the flow has been expanded and accelerated to $\vec{v}_2$ and angle α_2.

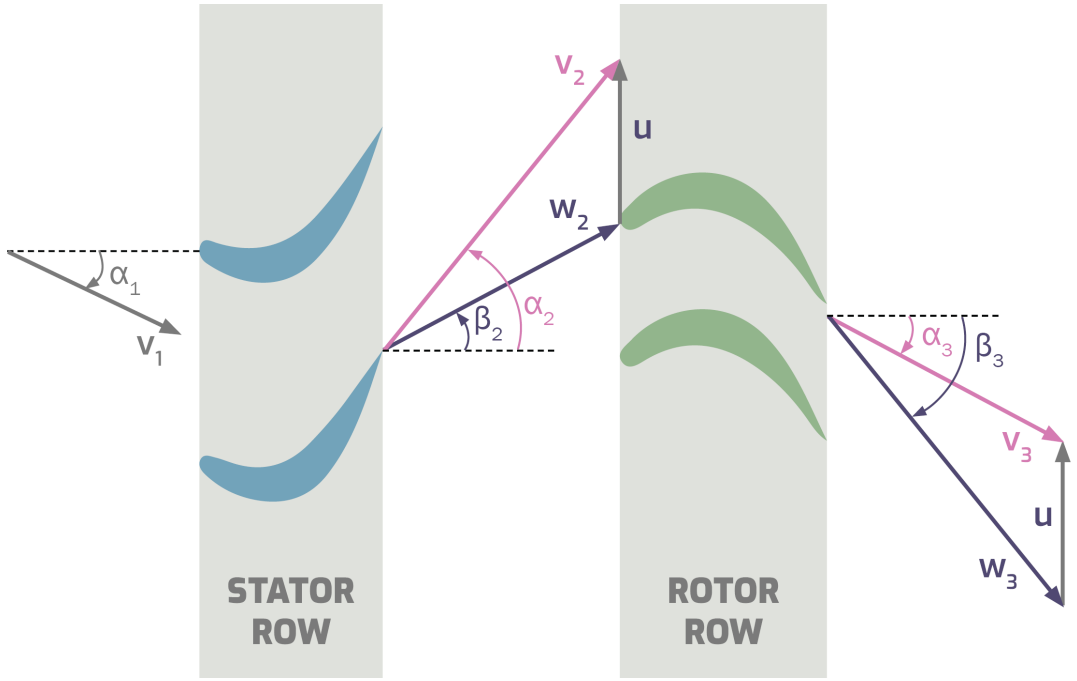

Figure 2.2: Diagram of velocity triangles in a turbine stage

Entering the rotor, the relative velocity is found by subtracting the blade velocity from the flow's absolute velocity:

$$\vec{w_2} = \vec{c_2} - \vec{u} \tag{2.2}$$

This velocity has an angle β_2. Since the blade velocity is purely tangential, the axial velocity of the flow does not vary: $v_{2x} = w_{2x}$.

At the rotor exit, the blade velocity is added to the relative velocity to find the absolute velocity, and the relative exit angle β_3 becomes the absolute exit angle, α_3:

$$\vec{v_3} = \vec{w_3} + \vec{u} \tag{2.3}$$

2.2 Turbomachinery and thermodynamics

References used in this section: Mattingly [8], Farokhi [5]

2.2.1 Fundamentals of turbine expansion

In a gas turbine engine, the purpose of the turbine is to drive the compressor. Thermodynamically, the turbine extracts work from the airflow as it exits the combustion chamber with high pressure and temperature. As the flow expands in the turbine, the pressure decreases, and the kinetic energy of the flow is converted to mechanical energy in the form of the rotation of the engine's shaft–which in turn causes the compressor to increase the pressure of air entering the engine.

Mattingly [8] uses the analogy of a pinwheel for a turbine: both essentially rotate due to a high-pressure inlet flow. And just as the pinwheel will not rotate at certain incidence angles, the blade shapes and turning angles must be carefully selected for optimal performance–one of the principal purposes of this design tool is to determine the best angles for the rotor and stator.

Figure 2.3: CHANGE IMAGE A pinwheel is analogous to a turbine.

A gas generator engine may be composed of several turbine stages, each connected to a compressor stage, and which are referred to as high-pressure and low-pressure turbines. In this project, the design is centered on an individual turbine stage–which can be used as a single-stage turbine, or as the initial section of several stages in a high-pressure turbine, as needed. A turbine stage is essentially made up of two components: the **stator** and the **rotor**.

Note: as described in section section 2.2.2, the degree of reaction defines the expansion completed in each stage. For the purposes of this document as well as the design tool, the turbine under consideration is a reaction turbine–that is, the flow is expanded in both the stator and the rotor.

Stator

The **stator** (also known as vane or nozzle) adapts the flow to a desired entry angle for the following rotor stage. The entry angle to the stator, for a single-stage or for the fist stage in a multi-stage turbine, is assumed to be axial and typically swirl-free [5]. The inlet angle α_1 therefore, is ideally 0, aligned with the turbomachinery axis. It is the rotor which imparts swirl–in other words, tangential velocity–to the flow.

Additionally, the first stage of turbine expansion is completed here. The total enthalpy conservation assumption is generally adopted–that is, the expansion in the stator (so long as the cooling is ignored, and the heat flux to blades and casing is assumed to be negligible)

is adiabatic. The total temperatures are conserved: $T_{01} = T_{02}$. The static pressure P decreases, as does the temperature T, whereas the velocity v increases dramatically.

$$\begin{aligned} P_1 > P_2 \quad &\longrightarrow \quad \Delta P < 0 \\ v_1 < v_2 \quad &\longrightarrow \quad \tfrac{\Delta v^2}{2} > 0 \\ T_1 > T_2 \quad &\longrightarrow \quad \Delta T < 0 \end{aligned} \tag{2.4}$$

In reality, the total enthalpy is not completely conserved, since there will always exist a heat flux between the airflow and the blades and casing. This

Rotor

The rotor receives the flow as it exits the stator (stage 2) the extracts work from the flow energy. As the flow expands through the rotor blades, it exerts an aerodynamic force on the blades, and the rotational energy is conducted through the shaft to the compressor. The tangential velocity which was introduced by the stator is, therefore, reduced, eliminated, or even reversed by the rotor.

In the rotor, the assumption generally applied concerns the enthalpy in the relative frame, also known as rothalpy. Thus, the total rothalpy is assumed to be constant, which can be expressed in terms of the total relative temperature $T_{02r} = T_{03r}$. Thus, the static pressure decreases in the rotor, as does the velocity and the temperature as the flow expands.

$$\begin{aligned} P_2 > P_3 \quad &\longrightarrow \quad \Delta P < 0 \\ v_2 > v_3 \quad &\longrightarrow \quad \tfrac{\Delta v^2}{2} < 0 \\ T_2 > T_3 \quad &\longrightarrow \quad \Delta T < 0 \end{aligned} \tag{2.5}$$

Isentropic and real expansion, stage efficiency

The variations in the flow's thermodynamic variables can be represented on an enthalpy-entropy diagram, where the ideal isentropic expansion is one in which there is no increase in entropy, ergo without loses. Realistically, keeping with the second law of thermodynamics, the entropy must increase during the expansion. This is done partially in the rotor, and partially in the stator, as was discussed.

The difference between the isentropic temperature and the real temperature is represented by the efficiency. This is analogous to both the work generated in the turbine and the enthalpies, and can be calculated as follows:

$$\eta_{turbine} = \frac{\text{Real turbine performance}}{\text{Ideal turbine performance}} = \frac{W_{real}}{W_s} = \frac{h_{01} - h_{03}}{h_{01} - h_{03s}} \tag{2.6}$$

which, using the heat capacity of the mixed flow, can be converted to temperature:

$$\eta_{turbine} = \frac{T_{01} - T_{03}}{T_{01} - T_{03s}} \tag{2.7}$$

For each individual portion of the expansion, the efficiency can be defined as well:

$$\eta_{stator} = \frac{T_{02} - T_2}{T_{02} - T_{2s}} \qquad \eta_{rotor} = \frac{T_{03} - T_3}{T_{03} - T_{3s}} \tag{2.8}$$

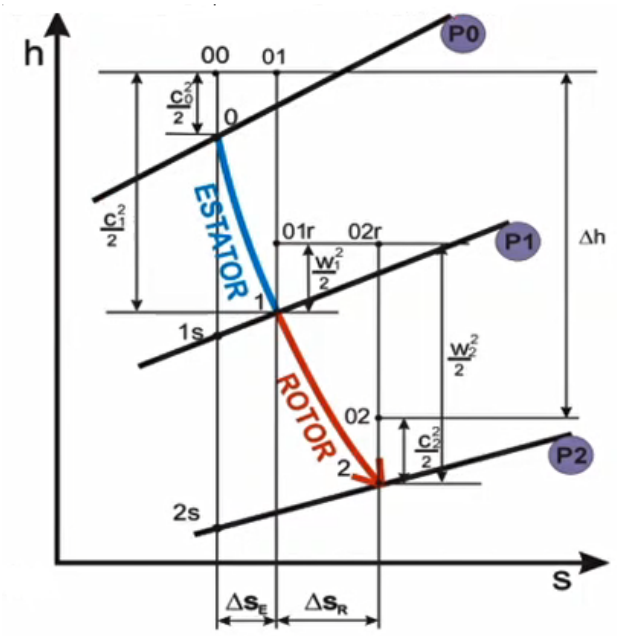

Figure 2.4: REMAKE FIGURE Isentropic vs. real expansion in a turbine stage

This value is the most practical figure for measuring the turbine's performance–the higher the efficiency, the lower the losses in the turbine, thus more work is extracted.

Energy extraction

The energy extracted from the flow by the rotor can be calculated through various methods, but the most powerful solution [5] is to apply Euler's turbine equation:

$$\Delta h = \frac{c_2^2 - c_3^2}{2} + \frac{w_3^2 - w_2^2}{2} + \frac{u_2^2 - u_3^2}{2} \tag{2.9}$$

In our case, since the peripheral speed is constant throughout the rotor (as will be discussed in the turbine model geometry), the equation can be simplified. Thus, Δh is found from the increase in axial velocity and multiplied by the peripheral speed, which is given by the angular velocity and the mean radius:

$$\Delta h = u\left(v_{2u} - v_{3u}\right) \tag{2.10}$$

In other words, the extracted energy is directly proportional to *how much the flow is accelerated in the rotor*. Intuitively, the extracted energy increases proportionally with the rotational velocity of the rotor, as well as with the mean radius.

2.2.2 Stage parameters

Degree of reaction GR: sometimes named $^{\circ}R$, the degree of reaction represents the expansion in the rotor compared to that of the entire stage. The definition [5] is given in

terms of the enthalpies of the stage:

$$GR = \frac{\Delta h_{rotor}}{\Delta h_{stage}} = \frac{h_2 - h_3}{h_1 - h_3} \tag{2.11}$$

Other definitions for the degree of reaction exit, and indeed the one which will be applied in this design tool is in terms of the stage static pressures [9]:

$$GR = 1 - \frac{1 - \left(\frac{P_2}{P_{01}}\right)^{\frac{\gamma-1}{\gamma}}}{1 - \left(\frac{P_3}{P_{01}}\right)^{\frac{\gamma-1}{\gamma}}} \tag{2.12}$$

whereas others use the relative and absolute velocities:

$$GR = \frac{w_2^2 - w_1^2}{w_2^2 - w_1^2 + v_0^2 + v_1^2} \tag{2.13}$$

Stage loading: The stage loading ψ represents the variation of enthalpy per turbine stage–it is a measure of how much work is demanded of a single stage. A high value of ψ indicates that each stage completes a large expansion–the requirements are higher, the required technology is more advanced, and the motor is more compact. Essentially, for a given stage, the pressure drop ΔP_0 increases with the stage loading.

Mathematically, the stage loading is equal to the specific work divided by the square of turbine non-dimensional blade speed.

$$\psi = \frac{\Delta H}{u^2} \tag{2.14}$$

High stage loading leads to higher swirl numbers and an increase in the Mach number, which could reduce efficiency factors. However, there is more work per stage, which can lead to fewer stages and reduction in weight and complexity.

Flow factor

The flow factor φ, also known as flow coefficient or flow function, is defined as the ratio of the axial velocity to the rotor speed:

$$\varphi = \frac{v_{1x}}{\Omega R_m} = \frac{v_{1x}}{u} \tag{2.15}$$

φ is ultimately a measure of how large a given gas turbine is, and inversely proportional to how fast the shaft rotates. This parameter, along with the stage loading factor, defines the Smith chart (see figure 2.5).

Loss parameters

The principal loss mechanism used in this project are the **pressure loss coefficients**, defined as the total pressure decrements referenced to the exit dynamic pressure, which represents

the loss of entropy in each stage. These are the parameters defined in [10] to estimate the losses quantitatively.

$$Y_{stator} = \frac{P_{01} - P_{02}}{P_{02} - P_2} \qquad Y_{rotor} = \frac{P_{02r} - P_{03r}}{P_{03r} - P_{3r}} \tag{2.16}$$

Note: this coefficient should not be confused with the total pressure loss coefficient.

Another parameter which is of interest is the **kinetic loss coefficient**, which represents the drop in enthalpy in terms of the exit energy:

$$\xi_{stator} = \frac{h_2 - h_{2s}}{\frac{1}{2}W_{2s}^2} \qquad \xi_{rotor} = \frac{h_3 - h_{3s}}{\frac{1}{2}W_{3s}^2} \tag{2.17}$$

Conversion of loss coefficients

At several points in the creation of this design tool, it has been necessary to use different references which use differing definitions for the loss coefficients. For example, the Kacker-Okapuu [10] model, from which most of the loss calculated have been applied, use the pressure drop in terms of the exit dynamic pressure, as seen in equation 2.16. On the other hand, may references, such as Denton [11] or Craig-Cox [12], use the kinetic loss coefficients defined in equation 2.17.

The conversion between these is relatively simple [13], although exact correlation is not achievable and differences appear in certain aspects of the design (for example, the pressure loss coefficients see a sharper increase with higher Mach numbers than the kinetic loss coefficients when compared to "neutral" parameters).

One equation which has been of use is the following: the calculation of a kinetic loss coefficient ξ from a pressure loss coefficient Y:

$$\xi = \left(\left(\frac{1+Y}{1+Y\left(P_2/P_{01}\right)} \right)^{\frac{\gamma-1}{\gamma}} - 1 \right) \left(\frac{1}{\left(P_2/P_{01}\right)^{\frac{\gamma-1}{\gamma}}} - 1 \right)^{-1} \tag{2.18}$$

2.2.3 Isentropic equations, Bernoulli equation, and ideal gas relation

Through the gas turbine engine, many isentropic and adiabatic relations are used to compute the ideal relations between stages–although the real values will be different.

For a calorically perfect gas undergoing an isentropic process ($s_1 = s_2$), the following equations must hold:

$$\frac{P}{P_0} = \left(\frac{\rho}{\rho_0} \right)^{\gamma} = \left(\frac{T}{T_0} \right)^{\frac{\gamma}{\gamma-1}} \tag{2.19}$$

$$\frac{P}{P_0} = \left(1 + \frac{\gamma+1}{2} M^2 \right)^{-\frac{\gamma}{\gamma-1}} \tag{2.20}$$

$$\frac{T}{T_0} = \left(1 + \frac{\gamma+1}{2} M^2 \right)^{-1} \tag{2.21}$$

$$T_0 = T_{dynamic} + T_{static} = \frac{V^2}{2C_p} + T \tag{2.22}$$

In the scope of this work, the airflow through the turbine (a mixture of atmospheric air and fuel, after combustion) is assumed to follow the ideal gas relation, permitting the usual relationship between the pressure, temperature, density, and specific gas constant:

$$P = \rho RT \tag{2.23}$$

2.2.4 Additional design considerations

Although many additional factors are at play within a turbine design, this design tool has a limited reach. Many crucial considerations are beyond the scope of the preliminary design proposed here, but are worth mentioning within the global overview of a turbine design proposal.

Loads upon turbine blades

A high-pressure turbine blade has a series of loads and tensions at work upon it from diverse sources: the principal culprits are aerodynamic forces and the exposure to high temperatures. These apply a variety of strains on the blades, in the form of mechanical loads, thermal loads, fatigue cycles, and vibrations, cooling requirements.

The mechanical loads are often at odds with the aerodynamic design of a turbine blade– for example, a slim trailing edge reduces losses due to turbulent wake, but on the other hand, the structural integrity of the blade is put into danger if the thickness of the trailing edge is reduced overmuch.

Cooling

One of the principal problems arising in turbine blade design is the cooling. The blade's theoretical models, as discussed in this report, meet the aerodynamic requirements for extraction of the work from the airflow. However, refrigeration is necessary to preserve the blade's integrity under the thermal and mechanical stresses of the high-pressure turbine.

The refrigeration of turbine blades is beyond the scope of this work, but the the existence of cooling systems may create constraints upon the calculations made in this design tool. For example, in trailing-edge thickness, blade maximum thickness, coatings, appearance of secondary flows, or other phenomena.

Maximum peripheral speed

The rotational velocity of the turbine is a crucial factor for work extraction, but is limited by the peripheral velocity u at the rotor tip. A high value of u causes high mechanical loads on the turbine blades. Excessive peripheral speeds may be promoted by increased rpms or enlarged turbine radius. This may be mitigated by increasing blade thickness, which increases both losses and weight–a compromise solution must be found, limiting tip radius, blade thickness, and rotational speed.

Smith's chart

A crucial tool in the preliminary portion of a turbine design process is the Smith chart, also known as Swindell diagram. This is a scattering of turbine efficiencies in an $x-y$ plot, where the axes hold the stage loading ψ and flow function φ.

A reference Smith chart can be seen in figure 2.5. Four extreme cases of turbine blades can also be seen represented, showing how the design parameters selected will modify the necessary angles and blade thickness.

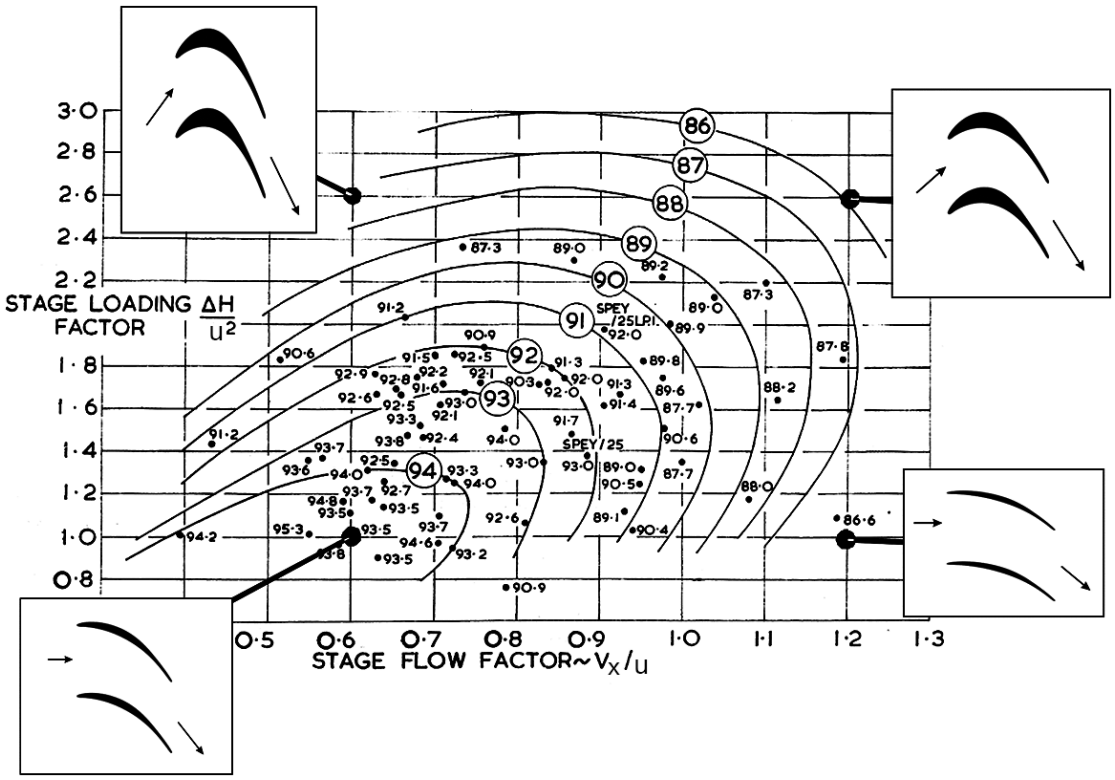

Figure 2.5: Smith chart featuring turbine efficiencies and representative turbine blades, adapted from [14]

The lower right-hand side of the diagram is where the focus of turbine design lies. This represents a moderate stage loading factor, and a very small flow factor: turbines in this area are small, but extract a lot of work. The classical get turbines, such as SPEY, have high stage loading and high flow factors.

A conservative design will have a moderate flow factor (will sit in the middle of the $x-$axis), but a small stage loading. A more compact, aggressive design will, for the same flow factor, have a higher stage loading–more work is extracted from each stage, for the same-sized turbine.

For the purposes of this design tool, a Smith chart may be useful to the user for selection of the stage loading within the preliminary design of the turbine.

2.3 Loss models

In conjunction with the theoretical evolution of the isentropic flow through a turbine, empirical correlations are used in the design tool to calculate the losses through the turbine stage. Based on the blade geometry, entry and exit pressures and velocities, these models can be used for calculation of the total loss–in this case, measured in the stagnation pressure loss coefficient–the total pressure loss with respect to the dynamic pressure.

All the loss correlations discussed in this section are applied to a 1-dimensional turbine model, or what is known as a mean-line model. Although 3-dimensional loss correlations (along the length of each blade) can be more accurate, the 1-dimensional models can be applied much earlier in the design cycle, before the complete blade geometry is determined, and providing an initial estimate of the turbine's efficiency.

2.3.1 Loss types

Denton [11] defines the sources of aerodynamic loss as viscous effects in boundary layers, viscous effects in mixing processes, shock waves and heat transfer across temperature difference. Although these are rarely uncoupled in practice [11], most loss correlation models are based on the initial models of the 1940's and 1950's. Thus, individual coefficients are calculated for each type of loss, and the total is a direct sum of these.

The individual classifications and calculations of loss, and the calculation of their coefficients, differs from author to author. Denton [11] identifies the principal three to be profile loss, endwall loss, and leakage loss, whereas other models (such as those based on the Ainley-Mathieson model [7]) define profile loss, secondary loss (which includes what Denton refers to as endwall loss, more extensively studied by Sharma and Butler [15], and the annulus loss). The Craig and Cox model [12] profile loss, secondary loss, hole loss, leakage, loss, and wire loss. The principal model followed in this project (Kacker-Okapuu, [10]) includes 4 distinct sources off pressure loss: profile, secondary, tip clearance, and trailing edge loss.

2.3.2 Kacker and Okapuu

The Kacker-Okapuu model, as described in [10], is a development of the Dunham-Came work [17], which is in turn an improvement of the Ainley-Mathieson method of performance estimation [7], possibly the most classic loss model used in turbine design. The Kacker-Okapuu model (hereafter referred to as *K-O*) is therefore based on an extensive quantity of experimental test data, and modified over time to follow the performance of existing turbines ever more closely. Most notably, the Kacker-Okapuu model introduces corrections for the effects of compressibility and shock waves at high Mach numbers, significantly improving the accuracy of the model at higher Mach numbers.

The K-O model has been reviewed extensively since its publication, for example in [13], [18], and [19]. While the results are often overestimated by all the common loss models [18], the K-O model hold up when compared to other, even more recent models, so long as a conventional gas turbine design is used. The results decay when the design has a low aspect ratio, or with large inlet flow angles. For the reach of this design program, as a tool for an initial analysis in a turbine design, this model is sufficiently close to the experimental results–

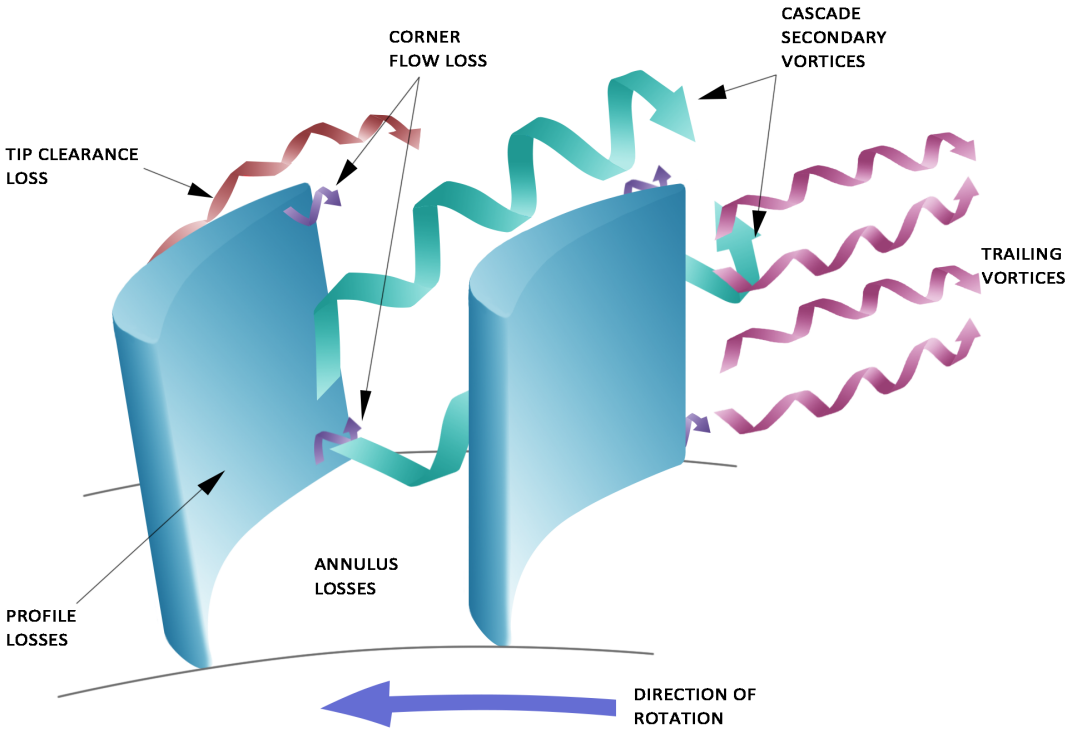

Figure 2.6: Representation of loss types, figure adapted from [16]

so long as the limitations are kept in mind. According to their original publication [10], this methods provides results accurate to $\pm 1.25\%$ in most turbine test cases.

The K-O method of loss estimation is based on an a series of linear cascade tests, supplemented by corrections from specific turbine and air tests [10]. As paraphrased from Farokhi [5], a cascade test consists of a series of two-dimensional or cylindrical blades placed in a uniform flow to simulate the two-dimensional flowfield about a spanwise section of a blade row. part from air tests.

The K-O model was selected for implementation in this design tool from among many loss models researched, most of which were mentioned in the previous section. Firstly, its position as one of the most common models used and reviewed in preliminary turbine analysis means that there is many reference sources available for use during this project. Secondly, this source offers all the primary losses (as discussed in the previous section) implemented in the same way: in terms of the pressure drop over each component. This significantly eases the integration of the model with the design tool. Finally, since all losses are determined by the same authors, any overlap between phenomena (where the same loss is calculated in two separate coefficients) is avoided.

In the K-O model, the pressure loss coefficient, defined as the total pressure loss over the exit dynamic pressure (see equation 2.16), is given as the sum of three terms:

$$Y = Y_P f_{\mathsf{Re}} + Y_S + Y_{TET} + Y_{TC} \tag{2.24}$$

Where each term represents the profile loss, secondary loss, trailing edge loss, and tip clearance loss, respectively. Additionally, the profile loss is ususally scaled by a factor f_{Re} which modifies the result according to the Reynolds number. Each of the individual loss models are discussed in the following sections.

Note: the equations in the following sections have been translated to the nomenclature followed in this report, which differs slightly from that used in the loss correlations reference documents.

2.3.3 Profile loss

Profile loss appears due to friction between the blade surface and the flow–that is, loss due to boundary layer interaction through viscous and turbulent dissipation, where mechanical energy from the flow is converted to heat. This phenomenon does not take into account the endwall interactions (since those are included in the secondary loss). It also excludes trailing edge losses, although other loss models such as Craig-Cox include these in the profile loss coefficient instead of a separate coefficient. The flow is assumed to be two-dimensional for this loss, so that cascade tests can be used to determine the necessary correlations.

The profile loss is directly defined by the boundary layer condition, which in turn depends on a variety of variables: pitch-to-chord ratio, Mach numbers, Reynolds number, blade geometry, and surface conditions, among others. In comparison to the previous models, the K-O model includes corrections for compressibility at high speeds, for shock losses, channel flow acceleration and supersonic drag rise.

Calculation of the profile loss coefficient Y_P

The profile loss coefficient Y_P, as proposed by K-O, is given by the following equation:

$$Y_P = 0.914 \left(\frac{2}{3} Y_{P,AMDC} K_P + Y_{shock} \right) \tag{2.25}$$

The term $Y_{P,AMDC}$ represents the profile loss coefficient as calculated with the Ainley-Mathieson model [7], as seen in equation 2.26.

$$Y_{P,AMDC} = \left(Y_{P(\alpha_{in}=0)} + \left| \frac{\alpha_{in}}{\alpha_{out}} \right| \left(\frac{\alpha_{in}}{\alpha_{out}} \right) \left[Y_{P(\alpha_{in}=\alpha_{out})} - Y_{P(\alpha_{in}=0)} \right] \right) \left(\frac{t_{\max}/c}{0.2} \right)^{\frac{\alpha_{in}}{\alpha_{out}}} \tag{2.26}$$

This equation represents an interpolation between two sets of cascade data: the coefficients $Y_{P(\alpha_{in}=0)}$ and $Y_{P(\alpha_{in}=\alpha_{out})}$, established by the original Ainley-Mathieson model [7]. Both are defined for the reference case of blade maximum thickness-to-chord ratio $t_{max}/c = 0.20$. These data sets provide the coefficient Y_P in terms of the pitch-to-chord ratio s/c and the outlet angle α_{out}. The data can be represented as a surface plot, as seen in figure 2.7.

The next value in equation 2.25 is the K_P correction factor, which is given by the following relation:

$$K_P = 1 - K_2 \left(1 - K_1 \right) \tag{2.27}$$

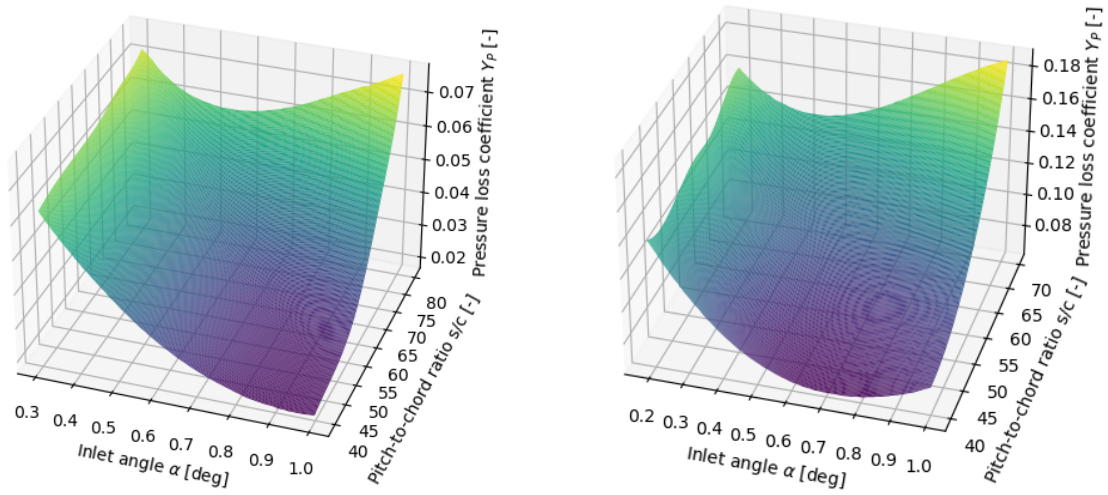

(a) $\alpha_{in} = 0$ (b) $\alpha_{in} = \alpha_{out}$

Figure 2.7: SWITCH X-Y AXES Surface plot of the profile loss coefficients for limit cases. Data from [7, 10]

This equation combines two factors which correct for high Mach exit numbers (K_1) and channel acceleration (K_2), compared to the low subsonic cascade test data represented in figure 2.7. These factors are represented in

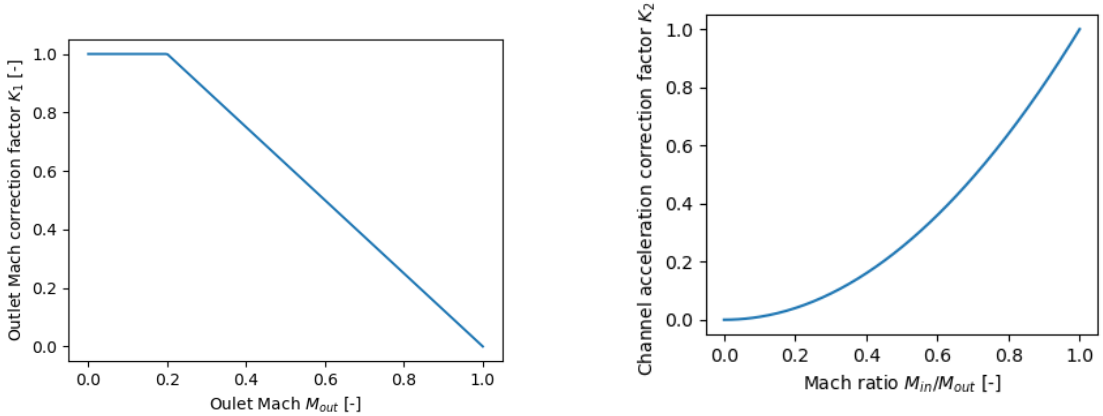

Figure 2.8: FIX FORMAT Mach number correction factors K_1 and K_2 for accelerating cascades, adapted from [10]

These factors, when included into equation 2.27, provide the Mach correction factor:

$$K_P = \begin{cases} 1 & \text{for} \quad M_{out} \leq 0.2 \\ 1 - 1.25 \left(\frac{M_{in}}{M_{out}}\right)^2 (M_{out} - 0.2) & \text{for} \quad M_{out} > 0.2 \end{cases} \tag{2.28}$$

The numerical factors in equation 2.25 represent corrections to the Ainley-Mathieson-Dunham-Came (AMDC) model as seen in [7,17], taking into account technological advances

and differences in formulation. The final term in the profile loss calculation is the shock loss coefficient at blade leading edge, Y_{shock}. This term is given as the pressure loss in terms of the inlet dynamic head, which is given at the mean line by the following relationship, dependent on inlet Mach and the tip to hub ratio:

$$\frac{\Delta P_{shock}}{q_{in}} = \frac{3}{4} R_{th} \left(M_{in,hub} - 0.4\right)^{1.75} \tag{2.29}$$

Finally, the shock loss coefficient must be translated to the blade exit dynamic head or q_{out} so as to be in the same reference as the remaining coefficients. This is done by applying the isentropic relation (equation 2.20) to equation 2.29:

$$Y_{shock} = \frac{\Delta P_{shock}}{q_{out}} = \frac{\Delta P_{shock}}{q_{in}} \frac{P_{in}}{P_{out}} \frac{1 - \left(1 + \left(\frac{\gamma-1}{2}\right) M_{in}^2\right)^{\frac{\gamma}{\gamma-1}}}{1 - \left(1 + \left(\frac{\gamma-1}{2}\right) M_{out}^2\right)^{\frac{\gamma}{\gamma-1}}} \tag{2.30}$$

Finally, and to complete the profile loss model, the correction for the Reynolds number must be defined–the term f_{Re} in equation 2.25. This is achieved with a piece-wise equation which represents the modification of the profile loss coefficient in comparison to Ainley-Mathieson's reference Reynolds number of $2 \cdot 10^5$ [7]. This relationship is quite similar to that proposed by Denton [11], although that formulation includes variation with blade surface roughness–which is beyond the limits of the current initial analysis. The results for a typical number of surface roughness, $K_S = 5 \cdot 10^4$ [11], follow the same trend (see figure 2.10).

$$f_{\mathrm{Re}} == \begin{cases} \left(\frac{\mathrm{Re}}{2 \cdot 10^5}\right)^{-0.4} & \text{for} \quad \mathrm{Re} \leq 2 \cdot 10^5 \\ 1 & \text{for} \quad 2 \cdot 10^5 < \mathrm{Re} < 10^6 \\ \left(\frac{\mathrm{Re}}{10^6}\right)^{-0.2} & \text{for} \quad \mathrm{Re} \geq 10^6 \end{cases} \tag{2.31}$$

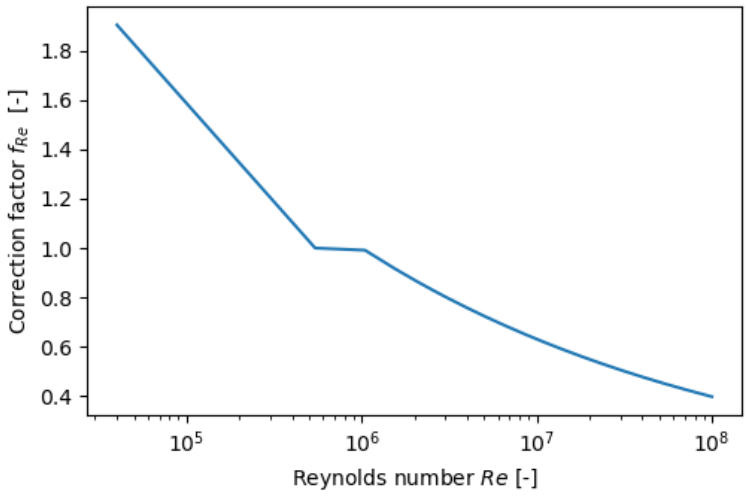

Figure 2.9: Reynolds number correction for profile losses, K-O model. Data from [10]

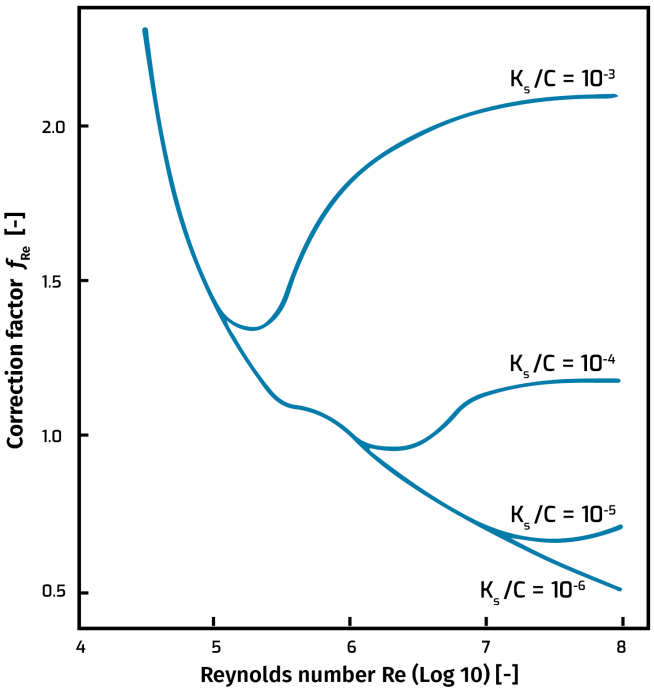

Figure 2.10: Reynolds number correction for profile losses (Denton model), in terms of the surface roughness K_S/C. Figure adapted from [11]

2.3.4 Secondary loss

The secondary loss stems from the interaction of the secondary flow with the main flow, the creation of vortices and interaction between them. In some cases, the secondary loss coefficient includes loss due to the synergy of the secondary flow with boundary layers. Within the K-O model, the annulus losses are classified in this coefficient as well.

Due to the 3-dimensional nature of the losses, the models cannot be constructed using cascade test data–Denton [11] considers this portion the most difficult of all to characterize and model. Thus, the calculation will be dependent on the entry and exit angles and Mach numbers, chord, and aspect ratio. This last parameter is the novelty introduced by K-O [10] in comparison to the previous model [17].

Calculation of the secondary loss coefficient Y_S

The secondary loss coefficient is defined by K-O [10] as the following:

$$Y_S = 1.2 Y_{S,AMDC} K_S \tag{2.32}$$

In the same way as the profile losses in the previous section, the K-O model introduces a few corrections to the previous models developed by [7, 17]. In this way, the original coefficient $Y_{S,AMDC}$ is defined as:

$$Y_{S,AMDC} = 0.1336 f_{AR} \frac{\cos^3 \alpha_{out}}{\cos \alpha_{in}} \left(\tan \alpha_{in} + \tan \alpha_{out}\right)^2 \frac{1}{\cos \alpha_m} \tag{2.33}$$

where the mean gas angle α_m is defined as:

$$\alpha_m = \arctan\left(\frac{1}{2}\left(\tan\alpha_{in} - \tan\alpha_{out}\right)\right) \tag{2.34}$$

and the term f_{AR} represents the correction for blade aspect ratio, or height-to-chord ratio, h/c, in a nearly-continuous function defined by K-O (figure 2.11):

$$f_{AR} = \begin{cases} \frac{1-0.25\sqrt{2-h/c}}{h/c} & \text{for} \quad h/c \leq 2 \\ \frac{1}{h/c} & \text{for} \quad h/c > 2 \end{cases} \tag{2.35}$$

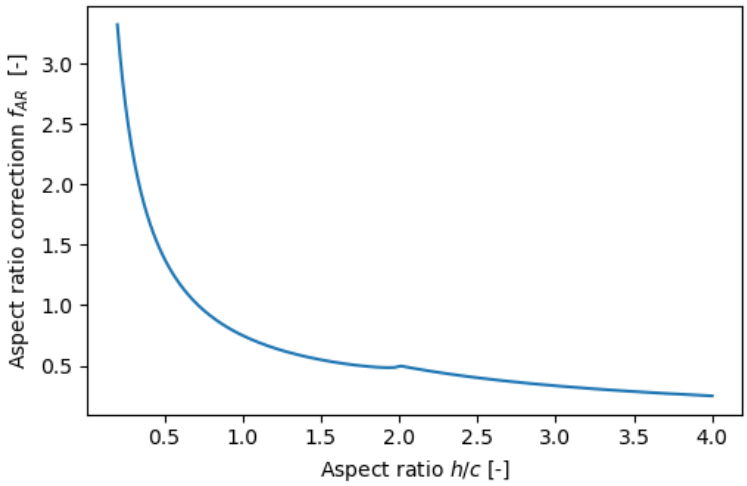

Figure 2.11: Aspect ratio correction factor, equation 2.35 from [10]

The factor of 1.2 which appears in equation 2.32 is due to the uncoupling of the secondary and the trailing-edge losses approached by the K-O model, which in the AMDC model were related through a multiplication of their coefficient.

Finally, the factor K_S is the subsonic factor correction which accounts for compressibility not included in the profile losses through Y_{shock}. This factor is defined by the following equation:

$$K_S = 1 - K_3\left(1 - K_P\right) \tag{2.36}$$

where K_P is the same Mach correction factor as defined in equation 2.28. K_3 is a factor in terms of the inverse of the height-to-axial-chord ratio, h/c_x, what could be considered the axial aspect ratio:

$$K_3 = \left(\frac{c_x}{h}\right)^2 \tag{2.37}$$

Therefore the secondary loss Mach correction factor is given by:

$$K_S = 1 - \left(\frac{c_x}{h}\right)^2\left(1 - K_P\right) \tag{2.38}$$

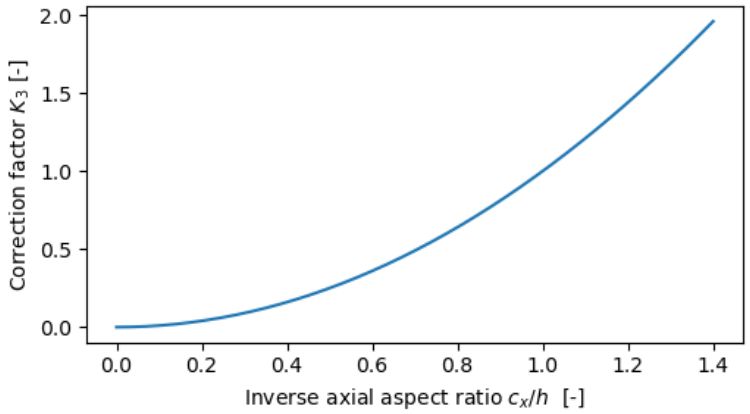

Figure 2.12: Subsonic Mach correction factor from axial aspect ratio, adapted from [10]

2.3.5 Trailing edge loss

The trailing edge losses appear due to the thickness of the blade at the trailing edge, and the subsequent flow separation and downstream mixing. Sharp corners may also introduce shock-expansion-waves [18]. This loss appears in significance in transonic and supersonic conditions–at lower Mach numbers, this loss is included with the profile loss.

Trailing edge loss can be established from cascade tests–in particular, the K-O model defines Y_{TET} in terms of the trailing edge thickness/throat opening ratio of a cascade [10]. Although the trailing edge loss presumably holds a dependence on the Mach number, it is not studied by K-O, who assume that the supersonic drag rise in case of exit velocities above $M = 1$ is included in the profile loss calculation.

Calculation of the trailing edge loss coefficient Y_{TET}

The trailing edge loss coefficients, as defined by the K-O model, are in terms of an energy coefficient $\Delta\phi^2$. Similarly to with the profile losses, the value of $\Delta\phi^2$ is defined for an axial entry $\alpha_{in} = 0$ and impulse blading $\alpha_{in} - \alpha_{out}$ by the set of experimental cascade data represented in figure 2.13. where t_{et} is the blade thickness at the trailing edge, and o_t represents the throat opening. Working off of this data, the energy loss coefficient can be calculated interpolated for different entry angles using a simple equation:

$$\Delta\phi^2 = \Delta\phi^2_{(\alpha_{in}=0)} + \left|\frac{\alpha_{in}}{\alpha_{out}}\right| \left(\frac{\alpha_{in}}{\alpha_{\text{out}}}\right) \left(\Delta\phi^2_{(\alpha_{in}=0)} - \Delta\phi^2_{(\alpha_{in}=\alpha_{out})}\right) \tag{2.39}$$

Once the energy coefficient is calculated, the loss is converted to a pressure coefficient using the isentropic relations from equations 2.16 and 2.20.

$$Y_{TET} = \frac{\left(1 - \frac{\gamma-1}{2} M^2_{out} \left(\frac{1}{1-\Delta\phi^2} - 1\right)\right)^{-\frac{\gamma}{\gamma-1}} - 1}{1 - \left(1 + \frac{\gamma-1}{2} M^2_{out}\right)^{-\frac{\gamma}{\gamma-1}}} \tag{2.40}$$

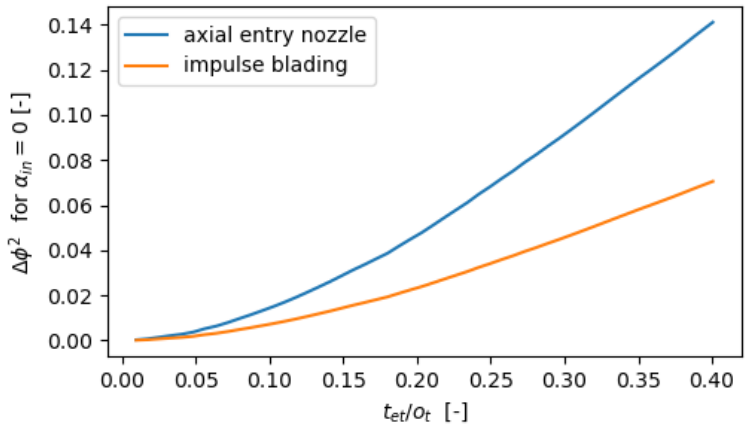

Figure 2.13: Trailing edge energy loss coefficient $\Delta\phi^2$ correlated to the trailing edge thickness to throat ratio t_{et}/o_t, adapted from [10]

2.3.6 Tip clearance loss

Tip clearance loss, also known as leakage loss, is found at the blade tips, where the clearance space between the blade edge and the rotor casing, or between the stator and turbine shaft. When the leakage flow is reintroduced to the main flow, the difference in velocities introduces mixing losses [18]. In addition, the leakage over the blade tip changes the massflow through the passages, which would in turn decrease the total work, modifying the global turbine parameters–although this effect has not been included in this design tool [20].

The tip clearance loss is fundamentally different in the case of shrouded or unshrouded turbine blades. In the case of unshrouded blades, the loss due to tip leakage can be up to $1/3$ of the total loss for the stage [21]. While the tip leakage is variable and can even be as high for shrouded blades for small turbines, in larger turbines the leakage, and therefore the loss, is much lower for shrouded blades [22]. Additionally, the massflow loss is reduced with shrouded blades, and therefore the drop in work produced by the rotor is lower [11]–although shrouded blades do suppose an increase in the turbine's mass and complexity.

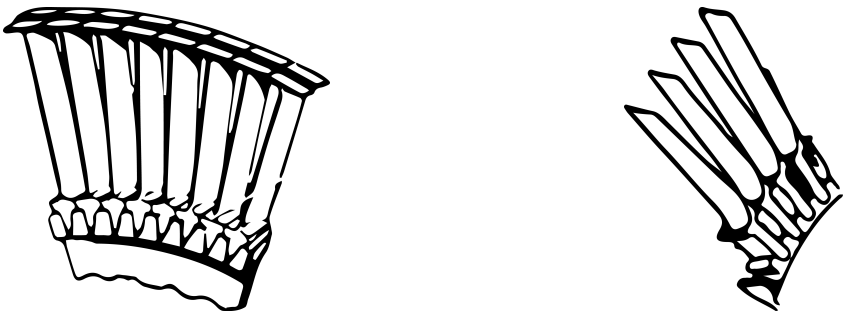

(a) shrouded tips

(b) unshrouded tips

Figure 2.14: Schematic diagrams of shrouded rotor blades (a) and unshrouded rotor blades (b), adapted from [21, 23]

Calculation of the tip clearance loss coefficient Y_{TC} with Denton model

Denton [11] proposes a different approach: by using the massflow of the leakage stream m_j (which passes over the blades), compared to that of the main stream m_1. In this way, the kinetic loss coefficient ξ for shrouded blades can be found with the following equation:

$$\xi = \frac{m_j}{m_2}\frac{e_{rel}}{e_2} = \frac{m_j}{m_2}\frac{V_{rel}^2}{V_2^2} \approx \frac{m_j}{m_1}\frac{V_{rel}^2}{V_1^2} = \frac{m_j}{m_1}\frac{V_x^2 + V_x^2\left(\tan\alpha_{out} - \tan\alpha_{in}\right)^2 + V_{jx}^2}{V_x^2 + V_x^2\tan^2\alpha_{out}} =$$
$$= 2\frac{m_j}{m_1}\left(1 - \frac{\tan\alpha_{in}}{\tan\alpha_{out}}\sin^2\alpha_{out}\right) \tag{2.41}$$

On the other hand, in the case of unshrouded blades, the tip loss coefficient is found through the following relationship of the inlet and exit angles:

$$\xi = \frac{2C_\delta\delta}{h}\int_{\tan\alpha_{in}}^{\tan\alpha_{out}}\sqrt{1 - \frac{\left(-\sqrt{c_1/3c_2} + \sqrt{1+x^2}\right)^2}{\left(\sqrt{c_1/3c_2} + \sqrt{1+x^2}\right)^2}}dx, \tag{2.42}$$

where

$$c_1 = \frac{1}{4}\left(\frac{\tan\alpha_{out}}{\cos^3\alpha_{out}} - \frac{\tan\alpha_{in}}{\cos^3\alpha_{in}} + 3c_2\right) \tag{2.43}$$

$$c_2 = \frac{1}{2}\left(\frac{\tan\alpha_{out}}{\cos\alpha_{out}} - \frac{\tan\alpha_{in}}{\cos\alpha_{in}} + \ln\frac{\tan\alpha_{out} + \frac{1}{\cos\alpha_{out}}}{\tan\alpha_{in} + \frac{1}{\cos\alpha_{in}}}\right) \tag{2.44}$$

The resulting kinetic loss coefficients, for both shrouded and unshrouded blade tips, can be seen in figure 2.15.

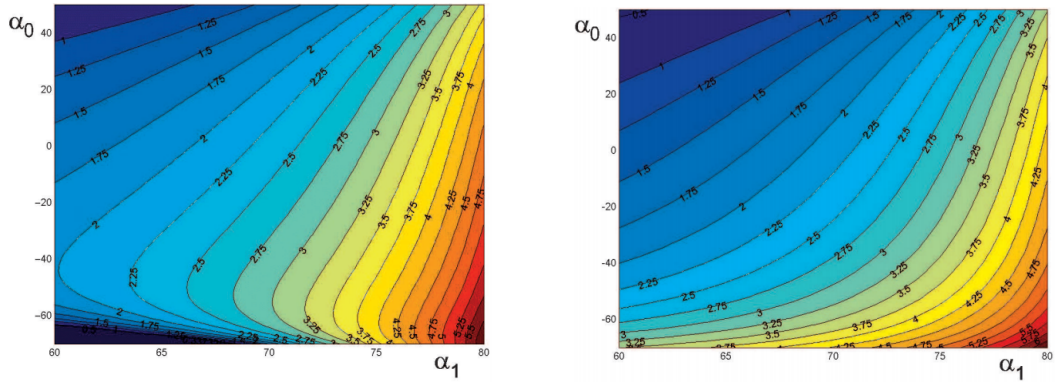

(a) shrouded tips (b) unshrouded tips

Figure 2.15: Loss coefficients (in % of kinetic loss) for tip leakage in shrouded (a) and unshrouded (b) blades, using the reference values $\delta = 0.01h$ and $C_\delta = 0.4$ from [24]

However, in the case of the current design tool, the parameters needed for the calculation of the loss coefficients following this method are specific to the blade geometry beyond the

preliminary scope of this project. The loss coefficients (taking into account the conversion to pressure loss coefficients, as seen in section 2.2.2) are much smaller than all the others taken into consideration in this work. Even in the extreme cases where α_{out} is high and α_1 is low, the kinetic loss coefficient is always inferior to the others due to the minimal clearance hypothesis adopted here, and therefore considered negligible in this work.

2.3.7 Limitations of the Kacker-Okapuu model

Although the original publication of the Kacker-Okapuu model [10] does not contain limitations or bound as to where it can be applied, subsequent studies and analyses have provided insights as to the range of validity of the model.

According to the analysis made by Lozza [13], the predictions made by the K-O model overestimate the losses once high Mach numbers are found at the rotor entry, $M_2 > 1.3$. This is due to the penalties introduced for expansion, which are accurate below this point.

The dependence of the K_S coefficient on the aspect ratio also introduces a strange singularity in the model, where anomalous trends appear if the aspect ratio h/c. Therefore the K-O model is unapplicable for impulse bladings with low aspect ratios ($h/c < 0.5$ [13].

Finally, the model has a limitation with very low deflection designs. For example, if $\alpha_1 = 140°$ and $\alpha_2 = 20°$, the profile losses become negative. This is only a problem in second stage turbines, such as an LP turbine which follows a high pressure turbine with a high swirl exit angle.

2.4 Software and code resources

The initial models of the program have been implemented in Python 3.8.5. This high-level programming language was selected due to its simplicity and relevance in the current aerospace industry, in addition to the facilities provided by existing libraries and packages for computational algorithms, optimization, and visual depiction of data and results.

The entire repository for the code used can be accessed at the following link:

`https://github.com/alosola/tfg/tree/master/code`

A brief summary of the libraries and functions used, as well as the appropriate citations, is included in this section.

2.4.1 Python libraries

Several open-source python libraries have been used in the design tool, containing both mathematical tools and visualization resources. Most of these are commonly used python libraries, although more specific tools have been applied in some cases and are worth discussing. All the code implemented in this project has been written by the author except the use of the libraries here mentioned.

Numpy [25] is the fundamental Python library for all the high-level mathematics in this design process. Based in C, it brings more powerful computational power to Python code. It is also the foundation for the additional libraries used.

Scipy [26] is based on Nympy, and contains many algorithms and functions for numerical data processing and solving. In particular, the `scipy.optimize` package contains several minimization and optimization functions which are used for non-linear problems in this program. Additionally, the `scipy.interpolate` package is used for processing of the experimental loss models.

Matplotlib [27] is a comprehensive library with all the necessary tools for visual representation of data: all figures, animations and data plots included in this document have been generated using this library. *** confirm this when finished ***

Pandas [28] is a data analysis and manipulation library, used in this program for tables and data visualization.

2.4.2 Optimization functions

The optimizations completed in the design tool have been completed with functions from the `scipy.optimize` package. A brief description of these is made here, in particular since the mathematical algorithms applied in these may have an effect on the results and/or computational speed.

`fsolve` part of the SciPy optimization package, this function is a Python wrapper for the `hybrd` function from the FORTRAN library MINPACK. In this algorithm, Powell's dog leg method is used to find the roots of a system of N non-linear functions [29]. This function is used for small multivariate convergence cases within the turbine calculations, such as the exit Mach convergence loop, as well as the global minimization in the open convergence case (section 4.2).

`least_squares` with the `trf` or Trust Region Reflective algorithm method. Also included in the SciPy optimization package, this function applies the least-squares method to find the minimum in a non-linear problem. In contrast to `fsolve`, this function allows the user to specify bounds for each of the variables under optimization.

`minimize` with the `trust-constr` option implements a trust-region interior point algorithm for constrained non-linear multivariate optimization. The exact method, described in [30], uses slack variables to solve inequality constraints. This optimization function is used for the constrained loss convergence problem (section 4.3), where acceptable limits are applied to several velocity and angular variables. `minimize` was selected as the most versatile optimization method implemented in the Scipy library, and in contrast to the other methods, the trust-region method is best suited to the non-linear inequality constraints at play in this program.

2.4.3 Front-end visualization and user interface

2.5 Project workflow

The methodology followed in the creation of the design tool contains 8 distinct steps, all of which were essential to create the final tool. These were not followed sequentially in every

case, overlapping and/or and feeding back when needed.

1. **Preliminary research** on high-pressure turbines and their design, as seen in section 2.2, as well as the various loss models which have been discussed in section 2.3. During this research, a large variety of sources were considered–notes are taken of each work, building a reference log and summary which was useful during the creation of the tool and the composition of this report.

2. **Initial turbine model** with no pressure loss calculation, with given entry conditions and thrust requirements, including a predefined value for the efficiency of stator and rotor. This model implements a mean-line 1-dimensional model and the usual thermodynamic calculations to determine velocities and geometry at each analysis point in the turbine. Some numerical optimization tools are implemented to automate the process for a variety of conditions.

3. Iteration on the initial model by including **pressure losses** as a function of the blade angles and geometry. Introducing the models discussed in section 2.3, the resulting pressure loss is compared to the value given by the turbine model and the process repeated until a convergence is found and the values for rotor and stator efficiency determined.

4. Comparison of the **results** provided by the design tool for selected test cases, experimental and expected results.

5. **Design tool analysis and conclusion**.

Chapter 3

Turbine Model

3.1 Overview

The basis of the design tool will be the turbine model, a calculation tool which completes the necessary iterations to solve for all the interior variables. Given the basic inputs and constraints, the model can run through the thermodynamic and geometric variables for the two turbine components, stator and rotor, and completely determine global geometry, velocities, pressures temperatures, etc. for each point.

For this initial analysis, a 1-dimensional mean-line model for the turbine is selected. This allows the program to apply relatively simple equations to predict the results and efficiency of the turbine, without increasing the complexity of the design much beyond what can be found in many textbooks [31].

For a description of the planes and nomenclature, please see section 2.1.1.

3.1.1 Definition of geometry

The basic shape of the turbine must be pre-defined within the design tool, since the geometric calculations are included in the thermodynamic equations, as well as the loss calculations.

In this case, a variable tip-and-hub configuration is selected, where the radius of both tip and hub is constant in the stator, whereas the rotor has a diverging shape: the radius of the tip is larger at the outlet than at the middle stage, and the radius at the hub is smaller, so that the cross-section of the rotor represents a trapezoid-like plane section (see figure 3.1). In this way, the mean radius R_m is constant in the whole stage, which is a convenient way to make the peripheral speed $u = \Omega R_m$ constant in the rotor–which simplifies the calculations made in the program.

Moving in closer, the relevant radii can be defined: R_t marks the tip (the outer edge of the blades), R_h the hub (where the blades meet the shaft), R_m the mean radius for that section. h represents the blade height.

3.1.2 Inputs

The design tool needs only a limited number of input values: inlet and outlet temperatures and pressures, as well as the enthalpy required of the turbine. These can be deduced from a

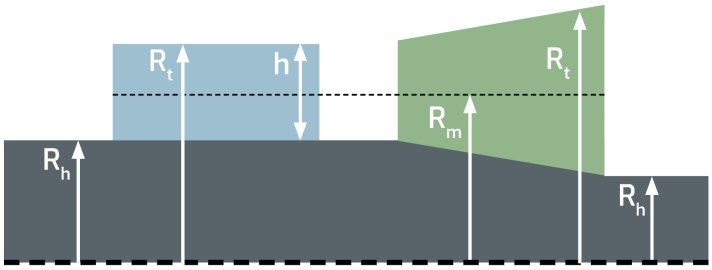

Figure 3.1: Geometry of turbine cross section.

global cycle analysis, or from the constraints imposed directly on the turbine by manufacturer.

Note: although this design tool is prepared for use of these parameters, the code may be modified with only slight alterations to the upper layers for application with different input variables, or else these parameters could be calculated directly from available values.

Table 3.1: Input parameters

Input parameter		Unit
Inlet: total temperature	$T01$	K
Inlet: total pressure	$P01$	Pa
Outlet: total temperature	$T03$	K
Outlet: total pressure	$P03$	Pa
Turbine enthalpy	ΔH_{prod}	$\mathrm{J\,kg^{-1}}$
Mass flow	$\dot{m}$	$\mathrm{kg\,m^{-3}}$

It should be noted that ΔH_{prod} represents the energy which must be produced by the turbine–this can be found by analyzing the compressor of the given generator, or through similar turbine designs.

Additionally, the user must select several **design parameters**, defining the type of turbine and performance expected. For this, several of the stage parameters defined in section 2.2.2 are used.

First, a degree of reaction GR is selected. This value, as discussed in section 2.2.2, represents the expansion in the rotor compared to the total expansion in the turbine stage. A higher value for GR will, in general, reduce losses and lead to better performance. However, as GR increases, so necessarily does the rotational speed in the rotor–this may lead to divergence and lower overall performance, and it is not recommended to have a GR greater than 0.6 [5].

On the low end of the scale, it is recommended for GR to be above 0.3 in value, where the low values are sometimes selected to increase the velocity in the stator and reduce the rotor inlet relative velocities, thus reducing the static pressure and the blade metal temperature [32].

The stage loading factor ψ is usually restricted to a range of 0.3-0.5 in modern high-pressure turbines [8, 32].

The tip to hub ratio R_{ht} selected at this point defines the geometry of the design–it should be within the range of 0.5-0.85. A low R_{ht} minimizes secondary losses, whereas a high R_{ht} reduces the tip clearance losses [32].

Table 3.2: Design parameters

Design parameter		Unit
Degree of reaction	GR	-
Loading factor	ψ	-
Tip-to-hub ratio	R_{ht}	-

3.1.3 Outputs

*** completar *** A number of variables are calculated within the design tool: both thermodynamic quantities, used in the models and calculations, and geometric values, translating the numerical solutions to a visual model.

All of these values could be extracted form the design tool as output, if desired. In this case, the selected outputs are shown in **??**. In addition, graphs for the velocity triangles, pressure and temperatures, and models of the turbine geometry are generated. *** complete when finished ***

3.1.4 Assumptions and constants

A small number of assumptions are made in addition to the hypotheses and models discussed previously. This is done to limit certain variables to reasonable ranges, or to fix parameters which will be included in the optimization in the next chapter of the design tool. Thermodynamic constants and fuel characteristics must also be defined.

First, it should be noted that the stator inlet angle is fixed to zero $\alpha_1 = 0$ in this program. That is, the flow is assumed to be purely axial for the purposes of this design program, since the turbine stage under design is meant to follow the combustion chamber directly, as was discussed previously.

In particular, the thermodynamic efficiencies of both stator and rotor must be assumed at this point. *** find reasonable numbers and references ***

The highest efficiency for the total stage in the best designs is about 0.95 [32].

Table 3.3: Turbine design assumptions

Parameter		Unit
Stator efficiency	η_{stator}	-
Rotor efficiency	η_{rotor}	-

The thermodynamic constants needed in the design tool can be seen in Table 3.4. These can also be modified when the design tool is run, if the fuel mix used is different to the standard–these values refer to the air-and-fuel mix which exits the combustion chamber. ** add references from Fletcher ***

Table 3.4: Thermodynamic constants

Parameter		Default value	Unit
Heat capacity ratio	γ	1.3	-
Heat capacity	C_p	1240	$\mathrm{J\,K^{-1}}$
Specific gas constant	R	286.15	$\mathrm{J\,kg^{-1}\,K^{-1}}$

3.2 Convergence functions

The design tool, with the inputs described in section 3.1.2, will find one single solution for turbine stage–however this cannot be solved for directly. There are a number of parameters which can only be found using an initial guess and subsequent iterations until convergence is found, with the acceptable ranges for each value defined. Rather than complete these processes by hand, as has been done in the past, these parameters have been fixed by use of non-linear solvers (as specified in section 2.4.1).

Using these, an initial guess is made for the needed value (although, as will be seen later on, the results are insensitive to guesses within a large range of reasonable values). Next, the non-linear solver is applied to these functions, a convergence point is applied (where the final calculated value meets the initial guess), and the results extracted.

3.2.1 Outlet Mach

The first such parameter, on which all the subsequent calculations depend, is for the **outlet Mach number** M_3. Once this value is calculated, the outlet conditions are given, and using the reaction degree the middle stage can be solved for as well. An initial guess is needed for this convergence–however nearly any value for subsonic flow, M_3, leads to the same convergence point in all tested cases.

Given a guess for $M_{3,init}$, the static pressure at the outlet is defined by using the isentropic equation which relates total pressure and static pressure by means of the Mach number (equation 2.20), solving for P_3:

$$P_3 = P_{03}\left(1 + \frac{\gamma+1}{2}M_{3,init}^2\right)^{-\frac{\gamma}{\gamma-1}} \tag{3.1}$$

An the static temperature T_3 is computed through the isentropic relation (equation 2.19):

$$\frac{T_3}{T_{03}} = \left(\frac{P_3}{P_{03}}\right)^{\frac{\gamma-1}{\gamma}} \tag{3.2}$$

Intermediate plane

Since a value for GR has been assumed, the pressure ratio definition (equation 2.12) is applied to solve for the static pressure in the intermediate plane:

$$P_2 = P_{01}\left(1 + (GR-1)\left(1 - \left(\frac{P_3}{P_{01}}\right)^{\frac{\gamma-1}{\gamma}}\right)\right)^{\frac{\gamma}{\gamma-1}} \tag{3.3}$$

Once this pressure is found, the pressure in each of the planes has been determined. Next, the remaining variables in plane 2 are found. For this, it is necessary to assume an isentropic evolution in the stator. Since there is no rotation in the stator, no work is applied by the flow, and therefore the total temperature is constant, and because the total temperature at inlet is a design input:

$$T_{02} = T_{01} \tag{3.4}$$

The ideal static pressure T_{2s} can be found by applying the same isentropic flow relation as previously (equation 2.19) between planes 1 and 2:

$$T_{2s} = T_{02}\left(\frac{P_2}{P_{01}}\right)^{\frac{\gamma-1}{\gamma}} \tag{3.5}$$

Using the assumed stator efficiency, and the definition from equation 2.8, the real static pressure T_2 is easily found:

$$T_2 = T_{02} - \eta_{stator}\left(T_{02} - T_{2s}\right) \tag{3.6}$$

Next, the flow velocity is calculated by using the dynamic pressure (equation 2.22) and the temperature calculated in the middle plane:

$$T_{02} = \frac{v_2^2}{2C_p} + T_2 \qquad \longrightarrow \qquad v_2 = \sqrt{2C_p\left(T_{02} - T_2\right)} \tag{3.7}$$

The same equation can be used to calculate v_{2s} by substituting the ideal temperature:

$$v_{2s} = \sqrt{2C_p\left(T_{02} - T_{2s}\right)} \tag{3.8}$$

Once the static quantities have been calculated, the density ρ_2, speed of sound a_2, and Mach number M_2 of the stator exit are easily found:

$$\rho_2 = \frac{P_2}{RT_2} \qquad a_2 = \sqrt{\gamma R T_2} \qquad M_2 = \frac{v_2}{a_2} \tag{3.9}$$

3.2.2 Rotor inlet and outlet angles

At this point in the program, it is necessary to have the stator outlet α_2 and rotor outlet β_3 angles, so that the velocities can be projected along these axes, and the relative conditions calculated.

For a given set of angles, the program will perform a series of calculations (as follows) until the work produced can be calculated with the change in tangential velocity, as given

by Euler's turbine equation (2.10). This value is compared to the required ΔH produced by the turbine, and a set of angles selected which meets this criteria. Using the least squares method, convergence is found and the best angle combination selected.

*** the problem here is that we have two variables and only one condition to meet... so there could be several answers. Try 1. plotting results to see trends. or 2. Coming up with another condition. or 3. ? ***

The initial guess for α_2 and β_2, as well as the upper and lower bounds for each, are specified within the program. Because the results are sensitive to these parameters, the selection must be made with care. In addition, a larger entry angle (more tangential flow) will also increase the frontal area of the rotor, which is not desired. Applying limits from reference studies [], the limits can be set to $\alpha_2 \in [70°, 75°]$ for high pressure turbines. Equivalently, the rotor outlet angle can be fixed in this range: $\beta_3 \in [-65°, -60°]$.

Once an angle has been selected, the calculations are straightforward. First, the velocity at the intermediate plane v_2 is projected in axial and tangential components (respectively), using the angle α_2 as seen in figure 2.2:

$$v_{2x} = v_2 \cos \alpha_2 \tag{3.10}$$

$$v_{2u} = v_2 \sin \alpha_2 \tag{3.11}$$

Next, using the selected loading factor ψ, the peripheral speed in the rotor can be determined, applying the total change in enthalpy produced by the turbine (equation 2.14):

$$\psi = \frac{\Delta H_{prod}}{u_2^2} \qquad \longrightarrow \qquad u_2 = \sqrt{\frac{\Delta H_{prod}}{\psi}} \tag{3.12}$$

Relative conditions

Using this peripheral speed, the absolute velocities at plane 2 can be converted to relative velocities, taking into account the rotor's rotation. This is done by components, tangential and axial, since the peripheral velocity u Thus, according to equation 2.2, the relative velocity in the tangential plane is a simple subtraction:

$$w_{2u} = v_{2u} - u \tag{3.13}$$

whereas in the axial direction, the magnitude remains constant (perpendicular to $\vec{u}$):

$$w_{2x} = v_{2x} \tag{3.14}$$

and the total speed is easily found as the magnitude:

$$w_2 = \sqrt{w_{2u}^2 + w_{2x}^2} \tag{3.15}$$

The speed of sound at 2 is still the same as was computed in equation 3.9–therefore the relative Mach number M_{2r} is calculated. Necessarily, it will be much lower than the absolute Mach.

$$M_{2r} = \frac{w_2}{a_2} \tag{3.16}$$

The relative inlet angle is given by a simple trigonometric relation (see figure 2.2):

$$\beta_2 = \arctan \frac{w_{2u}}{w_{2x}} \tag{3.17}$$

Finally, to complete all values for the intermediate plane, the relative total properties are calculated using the relative Mach conditions (Equations 2.20 and 2.21):

$$T_{02r} = T_2 \left(1 + \frac{\gamma - 1}{2} M_{2r}^2\right) \tag{3.18}$$

$$P_{02r} = P_2 \left(1 + \frac{\gamma - 1}{2} M_{2r}^2\right)^{\frac{\gamma}{\gamma - 1}} \tag{3.19}$$

Rotor outlet

In its passage through the rotor, the flow maintains a constant rothalpy–therefore the relative total temperature s the same in the outlet as in the intermediate plane:

$$T_{03r} = T_{02r} \tag{3.20}$$

The isentropic evolution is calculated (equation 2.19), and using the rotor efficiency assumed at the outset, the static temperature at the outlet is calculated:

$$T_{3s} = T_{03r} \left(\frac{P_3}{P_{02r}}\right)^{\frac{\gamma - 1}{\gamma}} \tag{3.21}$$

$$\eta_{rotor} = \frac{T_{03r - T_3}}{T_{03r} - T_{3s}} \qquad \longrightarrow \qquad T_3 = T_{03r} - \eta_{rotor} \left(T_{03r} - T_{3s}\right) \tag{3.22}$$

Finally, just as was done for the intermediate plane, the relative velocities are calculated from the relative dynamic pressure:

$$T_{03} = \frac{w_3^2}{2C_p} + T_3 \qquad \longrightarrow \qquad w_3 = \sqrt{2C_p \left(T_{03r} - T_3\right)} \tag{3.23}$$

With the current guess value for β_3, the relative velocity w_3 can be projected into axial and tangential directions, respectively:

$$w_{3x} = w_3 \cos \beta_3 \tag{3.24}$$

$$w_{3u} = w_3 \sin \beta_3 \tag{3.25}$$

Since the peripheral speed is a function of the rotor's angular velocity Ω and the mean radius R_m, so long as the mean radius is constant, the peripheral speed will be constant:

$$u_3 = u_2 \tag{3.26}$$

Following the inverse method as was completed for plane 2, equation 2.2 can be applied to find the absolute tangential speed at the stator outlet:

$$v_{3u} = w_{3u} + u_3 \tag{3.27}$$

Once again, the axial component of the peripheral speed is 0, and therefore the relative axial speed is equal to the absolute axial speed:

$$v_{3x} = w_{3x} \tag{3.28}$$

which leads to the magnitude of the absolute velocity:

$$v_3 = \sqrt{v_{3x}^2 + v_{3u}^2} \tag{3.29}$$

Now all the outlet velocities have been determined, and the enthalpy produced can be calculated. This will be given by the work applied by the flow on the rotor:

$$\Delta H_{calc} = u_2 \left(v_{2u} - v_{3u}\right) \tag{3.30}$$

This value, referred to as *calculated enthalpy*, is the final value in this convergence loop, where the cost function is set to the difference between this value and the defined turbine enthalpy, where this value is set to be minimized by the convergence loop:

Rotor angle convergence: find α_2 and β_3 such that $(\Delta H_{prod} - \Delta H_{calc}) \to 0$

3.2.3 Outlet Mach (continued)

Once the angles and velocities for this iteration have been completed, and the rotor angles α_2, β_3 established, the convergence loop for M_3 can be completed.

First, the remaining outlet quantities are found. Once again, the density ρ_3, speed of sound a_3, and relative Mach number M_{3r} at the rotor outlet are easily found:

$$\rho_3 = \frac{P_3}{RT_3} \qquad a_3 = \sqrt{\gamma R T_3} \qquad M_{3r} = \frac{w_3}{a_3} \tag{3.31}$$

The absolute angle at outlet is also easily found though a trigonometric relationship:

$$\alpha_3 = \arcsin \frac{v_{3u}}{v_3} \tag{3.32}$$

Finally, the absolute Mach number is found using the absolute velocity:

$$M_3 = \frac{v_3}{a_3} \tag{3.33}$$

This value for outlet Mach is compared to the initial guess. The non-linear solver is integrated to find a solution for M_3 which, when set as the initial guess, provides a calculated value identical to the first.

Outlet Mach convergence: find $M_{3,init}$ such that $(M_{3,init} - M_3) \to 0$

Once the outlet Mach number has been defined, the total outlet conditions can be found with the isentropic equations:

$$T_{03} = T_3 + \frac{v_3^2}{2C_p} \tag{3.34}$$

$$P_{03} = P_3 \left(\frac{T_{03}}{T_3}\right)^{\frac{\gamma}{\gamma-1}} \tag{3.35}$$

The final step is to compute the loss coefficients for the rotor and stator. Two coefficients have been selected in this analysis, as mentioned in section 2.2.2. The pressure loss coefficients represent the change in total pressure divided by the dynamic head:

$$Y_{stator} = \frac{P_{01} - P_{02}}{P_{02} - P_2} \qquad Y_{rotor} = \frac{P_{02r} - P_{03r}}{P_{03r} - P_3} \tag{3.36}$$

Whereas the kinetic loss coefficients are:

$$\xi_{stator} = \frac{v_{2s}^2 - v_2^2}{v_2^2} \qquad \xi_{rotor} = \frac{w_{3s}^2 - w_3^2}{w_3^2} \tag{3.37}$$

3.2.4 Geometry and density

Once the outlet Mach number has been defined, and the intermediate conditions computed, the peripheral geometry of the stator and rotor can be defined.

Intermediate plane

For stage 2, the geometry is determined using the mass flow defined for the turbine and the axial velocity. Knowing that the following equation must be satisfied, the area A_2 is computed:

$$\dot{m} = \rho v_x A \tag{3.38}$$

Next, the assumed value for the hub–to-tip radius ratio is used to solve for both R_t and R_h:

$$R_{ht} = \frac{R_h}{R_t} \tag{3.39}$$

$$A = \pi \left(R_t^2 - R_h^2\right) = \pi R_t^2 \left(1 - R_{ht}^2\right) \tag{3.40}$$

The determination of the blade height, mean radius, and mean diameter are trivial:

$$h = R_t - R_h \qquad R_m = R_t - \frac{h}{2} \qquad D_m = 2R_m \tag{3.41}$$

Finally the angular velocity and rotational speed are easily found from the peripheral speed u:

$$\Omega = \frac{u}{R_m} \qquad RPM = \Omega \frac{60\,\mathrm{s}}{2\pi} \tag{3.42}$$

Stator inlet

At the stage inlet, a number of parameters must be determined before the geometry can be defined. The total density is calculated with the ideal gas relation (equation 2.23):

$$\rho_{01} = \frac{P_{01}}{T_{01} R} \tag{3.43}$$

For the static density, a simple local optimization is applied to find the correct value. This is completed using `fsolve`, where the initial guess for ρ_1 is slightly inferior to ρ_{01}.

For each iteration, given the current guess for ρ_1, the velocity at point 1 is calculated, using equations 2.19 and 2.22. This velocity is equal to the axial velocity, since the inlet angle α_1 is assumed to be 0.

$$v_1 = v_{1x} = \sqrt{2C_pT_{01}\left(1 - \frac{\rho_1}{\rho_{01}}\right)^{\gamma-1}} \tag{3.44}$$

With the velocity, the area can be found, using the mass flow and ρ_1 (as done in equation 3.38). This area is then compared to A_2: given the cylindrical nature of the stator, these areas must be equal:

$$A_1 = \frac{\dot{m}}{\rho_1 v_{1x}} = A_2 \tag{3.45}$$

Inlet density convergence: find ρ_1 such that $(A_2 - A_1) \to 0$

Next, the dynamic temperature is computed from the total temperature using equation 2.22, and the dynamic pressure with equation 2.19. The sonic conditions a_1 and M_1 are computed as was completed for the stage outlet.

Finally, and completing the geometry for the inlet, the same process is repeated as for plane 2 (reusing equations 3.38 through 3.41).

Rotor outlet

For the geometry at the rotor outlet, the density ρ_3 was computed previously in equation 3.31, and the axial velocity in equation 3.28. Since the massflow is also known, the area can be computed as was done previously:

$$A_3 = \frac{\dot{m}}{\rho_3 V_{3x}} \tag{3.46}$$

Since the mean radius R_m is equal for the entire rotor, this area can be defined as a function of the blade height at the rotor exit, allowing the determination of h_3:

$$A_3 = \pi\left(R_{3t}^2 - R_{3h}^2\right) \qquad \begin{aligned} R_t &= R_m + \tfrac{h}{2} \\ R_h &= R_m - \tfrac{h}{2} \end{aligned} \tag{3.47}$$

$$A_3 = \pi\left(\left(R_m + \frac{h_3}{2}\right)^2 - \left(R_m - \frac{h_3}{2}\right)^2\right) = 2\pi R_m h \tag{3.48}$$

$$h_3 = \frac{A_3}{2\pi R_m} \tag{3.49}$$

3.3 Summary of the initial turbine model

In summary, the initial model of the turbine is a 1-dimensional mean-line model which assumes the isentropic efficiencies for stator and rotor $\eta_{stator}, \eta_{rotor}$. Given these, program completes its process calculating the complete set of variables for each stage. This involves two local convergence cases, optimized for a quick solution, so that the work produced by the turbine equal to the desired value.

The problem with this proposal is, of course, that the stage efficiencies are assumed–although literature can be used to propose a reasonable value for stator and rotor efficiencies, the range of possible options is wide enough that the final design for the turbine may or may not coincide with a real case–it is possible for the divergence of the assumed efficiency from the real performance to be large enough that the preliminary design is useless.

Thus, in the next chapter, an alternative method will me proposed for the calculation of the efficiency: by introducing loss correlations. This will in turn adjust the input parameters, which will allow the program to calculate a much more accurate set of data for the given parameters and constraints.

Chapter 4

Integration of Loss Models

This section contains a summary of the implementation of the correlations described in section 2.3 intro the turbine model described in the previous chapter. For this, some additional parameters are calculated as well, and some additional hypotheses are taken. Next, the pressure loss coefficients are calculated and integrated into the turbine model with an optimization loop to find the true efficiency of the designed turbine. Finally, an alternative version is made where some constraints are placed on Mach numbers, flow angles, and geometrical parameters.

4.1 Calculation of pressure loss coefficient

Before the models discussed in section 2.3 can be implemented into the turbine design tool, several additional parameters must be discussed. First, a brief note on the notation used in the description of the loss models and the angles.

The subindices $\square_{in}$ and $\square_{out}$ are used in the definitions so as to not be confused with the sub-indices $1, 2, 3$ used in the turbine analysis. Thus, in the application of these correlations for each component, the following conversion is made:

$$\begin{aligned} \text{STATOR}: \square_{in} &\longleftrightarrow \square_1 \\ \square_{out} &\longleftrightarrow \square_2 \\ \\ \text{ROTOR}: \square_{in} &\longleftrightarrow \square_2 \\ \square_{out} &\longleftrightarrow \square_3 \end{aligned} \tag{4.1}$$

On the other hand, the angles referred to in the K-O model are written in this report as α_{in} and α_{out}. Although the reference document [10] marks the difference between the gas angle and blade angle, this only applies to turbines outside of design point. In out case, within the design point, the gas angles correspond exactly to the blade design angles, and therefore are interchangeable. Therefore, the angles have all been renamed α for simplicity, although they will correspond to absolute values in the stator and relative values in the rotor, such that:

$$\begin{aligned} \text{STATOR}: \alpha_{in} &\longleftrightarrow \alpha_1 \\ \alpha_{out} &\longleftrightarrow \alpha_2 \\ \text{ROTOR}: \alpha_{in} &\longleftrightarrow \beta_2 \\ \alpha_{out} &\longleftrightarrow \beta_3 \end{aligned} \tag{4.2}$$

In practice, the turbine will not always be operating at the design point–this causes the appearance of a real incidence angle, or gas angle, which modifies both absolute α and relative β incidence angles.

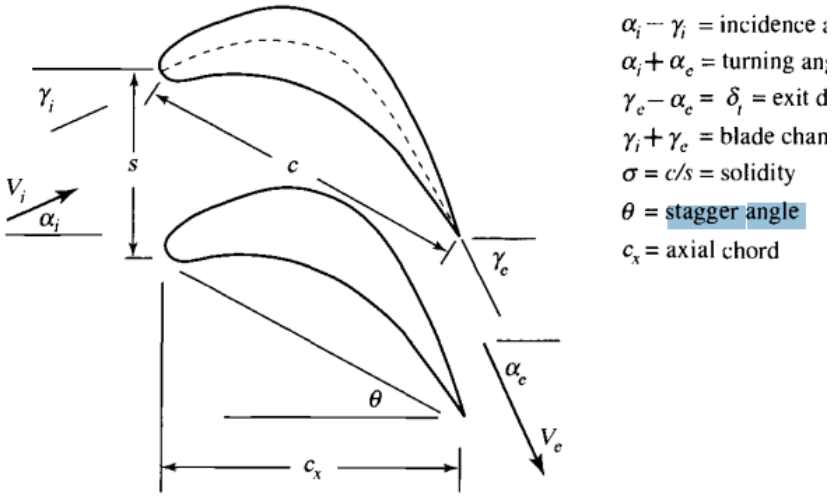

Figure 4.1: REMAKE FIGURE Representation of the angles in a turbine blade, adapted from [8]

4.1.1 Calculation of additional values

A number of additional parameters are not calculated by the initial turbine design tool, as discussed in chapter 3, and must be established before the loss models can be applied.

For the application of equation 2.26, all the angles are given by the turbine model, and the reference values extracted from the K-O model (see figure 2.7). The thickness-to-chord ratio t_{max}/c, if not specified by the user, can be calculated from a correlation found in [10] for typical turbine blade sections. This relation is represented in figure 4.2, and can be expressed numerically with the following piece-wise equation:

$$\frac{t_{max}}{c} = \begin{cases} 0.15 & \text{for} \quad \alpha_{in} + \alpha_{out} < 40° \\ 0.15 + 1.25 \cdot 10^{-3} \left(\alpha_{in} + \alpha_{out} - 40°\right) & \text{for} \quad 40° \leq \alpha_{in} + \alpha_{out} \leq 120° \\ 0.25 & \text{for} \quad \alpha_{in} + \alpha_{out} > 120° \end{cases} \tag{4.3}$$

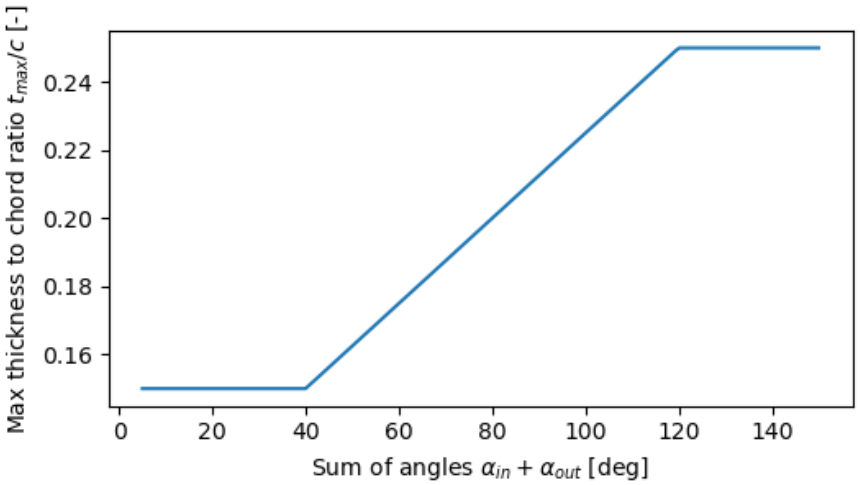

Figure 4.2: Max thickness/chord ratio for typical turbine blade sections, adapted from [10]

The inlet Mach number at the hub, as required by equation 2.29, is is given by [10]: for typical non-free-vortex turbines (represented in figure 4.3), the Mach at the hub is found in terms of the mean-line entry Mach M_{in}:

$$M_{in,hub} = \begin{cases} M_{in}\left(1 + 1.8 * (R_{th} - 1)^{2.2}\right) \text{ for stators} \\ M_{in}\left(1 + 5.2 * (R_{th} - 1)^{2.2}\right) \text{ for rotors} \end{cases} \tag{4.4}$$

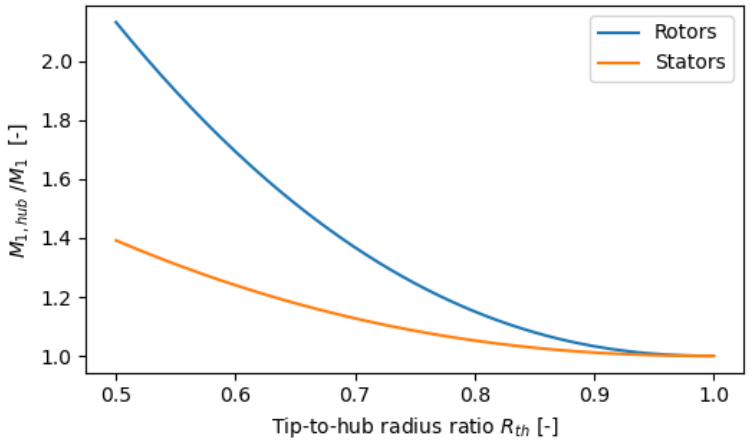

Figure 4.3: Inlet Mach number ratio from hub to mean-line from the tip-to-hub radius ratio, adapted from [10]

The blade chord c has not been defined by the turbine model. In practice, the height-to-chord h/c, also referred to as the aspect ratio in the loss models, is usually defined by the

user.

The axial chord can be found from projecting the chord c onto the shaft axis. The angle between these is the stagger angle ϕ, which the blade chord angle with respect to the axial direction [5] (as seen in figure 4.1). Thus, c_x is found:

$$c_x = c\cos\phi \tag{4.5}$$

The usual values of aspect ratio with axial chord, h/c_x, in a turbine are between 2.5 and 3.5, although higher values do exist [32].

The stagger angle ϕ is selected from reference turbines, in this case, a correlation provided by [10] (visible in figure 4.4). A function implemented in the design tool completes a bivariate spline approximation over a rectangular mesh provided in the reference document.

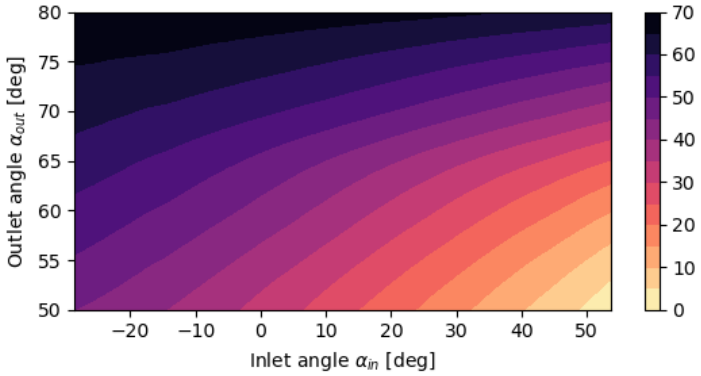

Figure 4.4: Contour map for the selection of stagger angle ϕ [deg], as selected from inlet and outlet angles. Data from [10]

The pitch s represents the distance between two turbine blades (see figure 4.1). The pitch can be determined through the Zweifel criterion [6]. Thus, the Zweifel blade-loading coefficient Ψ represents the ratio of the actual to the ideal tangential forces acting on the blade [16]. The equations is as follows:

$$\Psi = 2\frac{s}{c}\frac{1}{\cos\phi}\cos^2\alpha_{out}\left(\frac{V_{x,in}}{V_{x,out}}\tan\alpha_{in}+\tan\alpha_{out}\right)\frac{h_{out}}{h_{in}}\frac{P_{0,out}}{P_{0,in}} \tag{4.6}$$

By taking the Zweifel coefficient to be constant at the reference value of 0.8 for rotors, and 0.6 for stators [5], the pitch-to-chord ratio can be established. Since the chord has been determined previously, the pitch is also determined.

$$s = c\frac{\Psi}{2}\frac{\cos\phi}{\cos^2\alpha_{out}}\frac{\frac{h_{in}}{h_{out}}\frac{P_{0,in}}{P_{0,out}}}{\left(\frac{V_{x,in}}{V_{x,out}}\tan\alpha_{in}+\tan\alpha_{out}\right)} \tag{4.7}$$

where, as in the previous cases, the angles, velocities, and pressures are absolute in the stator, and relative in the rotor. Therefore, in the rotor, the variables at play in the equation are the relative variables: β, W_x, P_{0r}

The last variable which must be determined for the application of the loss models is the thickness-to-throat-opening ratio: t_{et}/o_t. This value, used in the calculation of the trailing edge loss, is difficult to determine from the available parameters, since the trailing edge thickness is a blade design parameter.

The throat opening o_t, on the other hand, can be determined from the spacing and entry angles. The formula for calculation of the throat takes into account the sonic throat A^* because of the possible appearance of supersonic flows (this equation, as referenced in [5], is applicable up to flows of $M \approx 1.3$). Once again, the values are applied to absolute values in the stator, and relative values in the rotor.

$$o_t \approx s \frac{\cos \alpha_{out}}{(A/A^*)_M} \tag{4.8}$$

Finally, the trailing edge thickness can be found from a correlation with the chord. Farokhi [5] states that the ratio between trailing edge thickness and mean blade chord, t_{et}/c, should fall between 0.015 and 0.05. A high value improves structural integrity and cooling access, whereas a small value increases the trailing edge losses and flow blockage.

Therefore, once the throat opening o_t is calculated and a t_{et}/c ratio selected, the t_{et}/o_t ratio is easily computed:

$$\frac{t_{et}}{o_t} = c \frac{t_{et}}{c} \frac{1}{o_t} \tag{4.9}$$

4.2 Integration of loss models with turbine model

The key to this convergence problem is the calculation of the pressure loss coefficients Y_{stator} and Y_{rotor}. This is done using equation 2.24, and all the additional functions described in that section, with some additional calculations described in the previous section. These resulting values are then introduced into the turbine model at the conclusion of the calculations represented in the previous model (once all the geometric parameters of all 3 planes have been established).

At this point in the model, we have the following calculated coefficients, each for both the stator and rotor:

1. An initial guess for the efficiency:

$$\eta_{stator},\ \eta_{rotor} \tag{4.10}$$

2. A pressure loss coefficient calculated with the definition (equation 3.36):

$$Y_{calc,stator},\ Y_{calc,rotor} \tag{4.11}$$

3. A pressure loss coefficient found using the correlation models (equation 2.24):

$$Y_{model,stator},\ Y_{model,rotor} \tag{4.12}$$

Using these values, we can use an optimization tool to find convergence. Applying the `fsolve` minimization function, the program uses the user-defined values for efficiencies η

to complete the calculations for the turbine model. Once these are complete, the calculated pressure coefficient is compared to that provided by the loss models. In the next iteration, the efficiency values are modified until convergence of the pressure loss coefficients is achieved.

Stator and rotor efficiency convergence: find $\eta_{stator}, \eta_{rotor}$ such that both $(Y_{calc,stator} - Y_{model,stator})$ and $(Y_{calc,rotor} - Y_{model,rotor}) \rightarrow 0$

This solution represents, therefore, a solution which predicts reality much more closely than the previous version of the model, since the pressure losses implied by the assumed efficiency coincide with those found by applying the loss correlations.

4.3 Addition of velocity and geometry constraints

The final feature added to the design tool is the addition of limiting constraints to the minimization loop. Thus, the final convergence is forced to lie within certain bounds which restrict the speed and angles within the turbine, providing a solution which is more realistic.

These constraints are implemented by creating a table of maximum and minimum acceptable values for the selected variables. This table is later included as a non-linear constraint in the `minimize` function, which completes the multivariate optimization. This process is analogous to that of the previous section, but with the addition of the constraints.

The constraints can be defined by the user at the initiation of a design process, with the remaining variables discussed in section 3.1, or left to the default values as discussed in the next sections. A summary of the constraints and example values is given in table 4.1

4.3.1 Swirl and angle constraints

The first constraints added correspond to the turning angles in the stator ($\Delta\alpha$) and rotor ($\Delta\beta$). These must be limited to $120°$, since high turning angles can increase the pressure loss due to secondary flows [5].

The exit swirl angle α_3 is dependent on whether or not there is a second stage immediately following the stage under design. If this is the case, the desired angle will in turn be in terms of the design of the low pressure turbine.

If the engine has a single-stage turbine, the swirl angle is important in performance. A low value, where $\alpha_3 \longrightarrow 0$, means that the exit velocity is nearly axial ($v_3 = v_{x,3}$) which minimized the kinetic energy of the flow. On the other hand, a high (that is, a high value of $-\alpha_3$, since the convention is for the exit to be backwards-running) increases the total magnitude of v_3, which in turn means that the stage output is greater [8]. According to Walsh-Fletcher, the swirl angle should ideally be zero but certainly less than $10°$ [32].

4.3.2 Mach number constraints

A few constraints must be placed on the Mach numbers in the various stages of the turbine. Mach numbers that are too high will cause shock waves and high values of kinetic loss, whereas low Mach numbers cause stage loading and flow factors outside the desired bounds. Also, the correlations in the loss models, as discussed in section 2.3.7, break down above a certain number.

The stator exit Mach number M_2 is generally restricted between between 0.75 to 1.2-1.3 [13,32]. The same is true of the relative Mach at the rotor exit, M_{3r}. On the other hand, the relative Mach at rotor inlet is restricted to 0.35–0.5, with 0.7 as an absolute upper limit. The absolute exit Mach number M_3 should not be higher than 0.35 and ideally 0.25 [32].

4.3.3 Additional constraints

A variety of additional constraints could be added to the design program.

Rim speed is of concern for blade and disc stress, but primarily impacts the last stage of a low-pressure turbine. Tip speed should be restricted for the sake of the disk and blade integrity, where it is limited to 400 m/s for titanium blades [32].

The relative angle at the rotor inlet β_2 should also be restricted to a range of $45° - 50°$.

The area ratio A_3/A_2 represents the increase in diameter apparent in the rotor. This value should be limited to decrease loss due to rapid divergence of annulus area, and additionally, the axial velocity of the flow would be reduced. While a value of around 1.2 is recommended as maximum, values of up to 1.35 can be accepted.

4.3.4 Limit checks

The limits described in the preceding sections are summarized into an array which is then fed into the design program as a variable, constraining the optimization of the efficiencies. The same limits are defined for the previous versions of the model–however they do not modify the results, and are simply available to the user for quick reference with the other results.

These values can easily be accessed and modified in the `limit_checks` submodule.

Table 4.1: Limits and constraints upon the turbine parameters

Parameter		Min	Max	Unit
Turning in stator	$\Delta\alpha$	0	120	°
Turning in rotor	$\Delta\beta$	0	120	°
Rotor relative entry angle	β_2	45	50	°
Exit swirl angle	α_3	0	10	°
Area ratio	$\frac{A_3}{A_2}$	1	1.35	-
Rotor inlet absolute Mach	M_2	0.75	1.3	-
Rotor inlet relative Mach	M_{2r}	0.35	0.7	-
Rotor outlet absolute Mach	M_3	0	0.35	-
Rotor outlet relative Mach	M_{3r}	0.75	1.3	-

4.4 Design tool versions

Once all the functions described in this chapter have been implemented, the design tool is complete. The result is a preliminary calculation tool which is useful for determining all the

general parameters in a turbine stage with straightforward calculations for narrowing design choices before more specific tools are applied.

The design tool, as presented here, has three versions:

1. **V1. No-loss model:** the first version of the tool, corresponding to the implementation seen in chapter 3. The thermodynamic variables are calculated for assumed efficiencies. In this model, only local convergence loops are completed (for M_3 and the rotor angles).
2. **V2. Losses (without limits):** the second version of the program incorporates the loss models and performs and optimization to find the true efficiency of the rotor and stator.
3. **V3. Losses (with limits):** the final version of the program includes the limits discussed in the previous section, utilizing these as constraints on the optimization process.

As can be expected, each of the versions is more complex, and therefore takes longer to compute, than the previous version. For a given problem, each of the versions can be run independently, using the same initial definition of variables. The output tables to each version are the same.

Chapter 5

Results, test cases, and validation

Once the preliminary research (chapter 2) and the implementation (chapters 3 and 4), the resulting design tool must be tested and validated to confirm that it functions correctly in the desired range of applications.

This has been done through two methods. First (section 5.1), several sample design cases have been selected from among existing turbines, as studied in previous research papers. This ensures that all the necessary input data is available, and that the results can be compared and validated.

The second portion of this chapter (section 5.2) contains a series of parametric analysis which were made using the design tool. By establishing a reference case and varying one parameter at a time, the effect of each variable upon the final results is analysed and compared to expected behavior.

The sample cases presented in this chapter, and calculated with the design tool, were performed using the second version of the design tool: that which includes the final convergence loop, but does not place constraints upon the velocities. This was selected because the additional constraints were not needed to find a viable solution in these cases, and the calculation time is significantly higher when the non-linear constraints are enforced. What is more, these values can sometimes impose artificial limits on values which need not be so strictly limited, and have therefore been monitored by the author for these cases.

The sample cases have been selected from various references, so as to compare the generated results to different design methods. Additionally, they have been selected in a range of turbine sizes, confirming the usability of the design tool for a range of turbine applications.

5.1 Sample design problems

5.1.1 Test case 1: Lyulka AL-21 High pressure turbine

The first test case implemented is that of the high-pressure turbine of the **LYULKA AL-21F3** axial flow turbojet engine. This is one of the engines used in the turbine design study completed by Ajoko [33], from which the necessary data has been extracted. All the necessary input parameters are described in that report, and displayed in table 5.1. Although some

differences exit between the geometry adopted in this design tool and the reference case (for example, the diverging shape of the rotor), the results will be compared and discussed.

Table 5.1: Inputs for test case 1

Parameter	Value	Unit
T_{01}	562.00	K
T_{03}	560.26	K
P_{01}	346.32	kPa
P_{03}	341.57	kPa
$deltaH$	0.18	MJ/kg
$mdot$	25.50	kg/s
GR	0.40	-
psi	2.06	-
R_{ht}	0.98	-

Using the input parameters, the design tool is run for this design case using the generic parameters as discussed in chapters 3 and 4. Once the calculations are complete, a summary of the results are displayed in a table as is done in [8] (table 5.2), and the resulting velocity triangle shown in figure 5.1.

This turbine is relatively small–the total thrust generated by the jet engine is 110 316 N [34]. Therefore the massflow through the engine is not extremely high, nor are the velocities reached (see figure 5.1) extremely elevated.

Table 5.2: Results for test case 1

Variable	Station					Unit
	1	2	2r	3r	3	
T_0	562	562	493.88	493.88	437.07	K
T	560.26	479.84	479.84	425.27	425.27	K
P_0	346.32	332.48	187.13	180.08	104.57	Pa
P	341.57	164.61	164.61	92.59	92.59	Pa
M	0.15	1.09	0.45	1.06	0.44	-
v	66.71	458.08	-	-	173.55	m/s
w	-	-	189.03	418.58	-	m/s
$alpha$	0.0	75.0	-	-	-0.6	deg
$beta$	-	-	51.16	-70.0	-	deg

The results in the turbine are as expected, with an expansion through both the stator and rotor. Some significant variables can be compared to the results of the reference study,

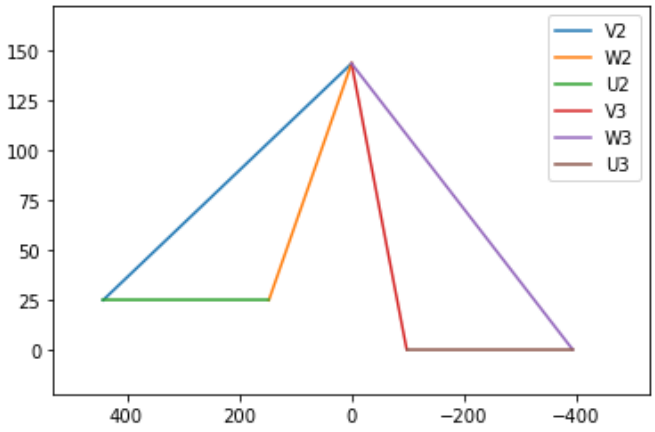

Figure 5.1: FIX AXES LABLES Velocity triangle for the turbine in test case 1

displayed here in table 5.3. As can be seen, the results are extremely similar to those of reference study, varying an average of 7.75% for the variables studied.

Table 5.3: Comparison of results for test case 1 to reference [33]

	eta_{tot}	phi	$DeltaT_0$	A3	h_2	u_m
Design tool	0.9	0.48	124.93	0.23	0.02	295.24
Reference	0.9	0.50	118.00	0.25	0.02	270.00

5.1.2 Initial stage of three-stage high-pressure turbine

5.1.3 Gas generator for automobile

5.2 Parametric analyses

5.2.1 Degree of reaction

5.2.2

5.3 Discussion

Chapter 6

Conclusion

(incluyendo, en su caso, líneas de trabajos futuros, y mencionando obligatoriamente las competencias –conocimientos y/o capacidades– del grado que el alumno ha aplicado al TFG y las nuevas competencias –conocimientos y/o capacidades– que el alumno ha adquirido con la realización del TFG)

6.1 Discussion of design tool creation and results

6.2 Personal growth

6.3 Future work

Bibliography

[1] Electricity explained. how electricity is generated. U.S. Energy Information Administration.

[2] John W.R. Taylor and John F. Guilmartin. Military aircraft: The jet age.

[3] Mukesh Yadav, Ashwin Misra, Aahan Malhotra, and Naveen Kumar. Design and analysis of a high-pressure turbine blade in a jet engine using advanced materials. *Materials Today: Proceedings*, 25:639–645, 2020. 2nd International Conference on Computational and Experimental Methods in Mechanical Engineering.

[4] Mohammad Arabnia. *Aerodynamic Shape Optimization of Axial Turbines in Three Dimensional Flow*. PhD thesis, Concordia University, 2012.

[5] Saeed Farokhi. *Aircraft Propulsion*. John Wiley & Sons Ltd, 2 edition, 2014.

[6] Rafael Guédez. Implementation and validation of loss prediction methods to an existing one dimensional axial turbine design program. Master's thesis, KTH School of Industrial Engineering and Management, 2011.

[7] D.G. Ainley, G.C.R. Mathieson, Aeronautical Research Council London (Great Britain), and Aeronautical Research Council (Great Britain). *A Method of Performance Estimation for Axial-flow Turbines*. Aeronautical Research Council. Reports and memoranda. H.M. Stationery Office, 1951.

[8] Jack D. Mattingly. *Elements of propulsion : gas turbines and rockets*. American Institute of Aeronautics and Astronautics, Inc., 2006.

[9] C.H. Sieverding. *Subsonic turbine blading design*. Von Karman Institute for Fluid Dynamics, 1985.

[10] S. C. Kacker and U. Okapuu. A mean line prediction method for axial flow turbine efficiency. *Journal of Engineering for Power*, 104:111–119, 1982.

[11] J. D. Denton. Loss Mechanisms in Turbomachines. *Journal of Turbomachinery*, 115(4):621–656, 10 1993.

[12] H. R. M. Craig and H. J. A. Cox. Performance estimation of axial flow turbines. *Proceedings of the Institution of Mechanical Engineers*, 185(1):407–424, 1970.

[13] Giovanni Lozza. A comparison between the craig-cox and the kacker-okapuu methods of turbine performance prediction. *Meccanica*, 17:211–221, 1982.

[14] S. Can Gülen. *Turbine Aero**, page 217–264. Cambridge University Press, 2019.

[15] O. Sharma and T. Butler. Predictions of endwall losses and secondary flows in axial flow turbine cascades. *Journal of Turbomachinery*, 109(2):229–236, 04 1986.

[16] Hany Moustapha, Mark F. Zelesky, Nicholas C. Baines, and David Japikse. *Axial and Radial Turbines*. Concepts ETI, Inc., 2003.

[17] P.M. Came J. Dunham. Improvements to the Ainley-Mathieson method of turbine performance prediction. *ASME Journal of Engineering for Power*, 92:252–256, 07 1970.

[18] Ning Wei. *Significance of Loss Models in Aerothermodynamic Simulation for Axial Turbines*. PhD thesis, Journal of KONES Powertrain and Transport, 2000.

[19] Daniel Back da Trindade, Pamela Bugała, and Domenico Simone. Review of loss models for high pressure turbines. *Journal of KONES Powertrain and Transport*, 25(2):211–221, 2018.

[20] F. J. G. Heyes, H. P. Hodson, and G. M. Dailey. The effect of blade tip geometry on the tip leakage flow in axial turbine cascades. *Journal of Turbomachinery*, 114:643–651, 1992.

[21] Z. Saleh, E. J. Avital, and T. Korakianitis. An investigation into turbine blade tip leakage flows at high speeds. *International Journal of Aerospace and Mechanical Engineering*, 7(1), 2013.

[22] M. Hamidur Rahman, Sung In Kim, and Ibrahim Hassan. Tip leakage flow and heat transfer on turbine blade tip and casing, part 1: Effect of tip clearance height and rotation speed. *International Journal for Computational Methods in Engineering Science and Mechanics*, 14(4):290–303, 2013.

[23] D. O'Dowd. *Aero-thermal performance of transonic high-pressure turbine blade tips*. PhD thesis, University of Oxford, 2010.

[24] Piotr Lampart. Tip leakage flows in turbines. *Task Quarterly*, 10:139–175, 01 2006.

[25] Charles R. Harris, K. Jarrod Millman, Stéfan J. van der Walt, Ralf Gommers, Pauli Virtanen, David Cournapeau, Eric Wieser, Julian Taylor, Sebastian Berg, Nathaniel J. Smith, Robert Kern, Matti Picus, Stephan Hoyer, Marten H. van Kerkwijk, Matthew Brett, Allan Haldane, Jaime Fernández del Río, Mark Wiebe, Pearu Peterson, Pierre Gérard-Marchant, Kevin Sheppard, Tyler Reddy, Warren Weckesser, Hameer Abbasi, Christoph Gohlke, and Travis E. Oliphant. Array programming with NumPy. *Nature*, 585(7825):357–362, September 2020.

[26] Pauli Virtanen, Ralf Gommers, Travis E. Oliphant, Matt Haberland, Tyler Reddy, David Cournapeau, Evgeni Burovski, Pearu Peterson, Warren Weckesser, Jonathan Bright,

Stéfan J. van der Walt, Matthew Brett, Joshua Wilson, K. Jarrod Millman, Nikolay Mayorov, Andrew R. J. Nelson, Eric Jones, Robert Kern, Eric Larson, C J Carey, İlhan Polat, Yu Feng, Eric W. Moore, Jake VanderPlas, Denis Laxalde, Josef Perktold, Robert Cimrman, Ian Henriksen, E. A. Quintero, Charles R. Harris, Anne M. Archibald, Antônio H. Ribeiro, Fabian Pedregosa, Paul van Mulbregt, and SciPy 1.0 Contributors. SciPy 1.0: Fundamental Algorithms for Scientific Computing in Python. *Nature Methods*, 17:261–272, 2020.

[27] J. D. Hunter. Matplotlib: A 2d graphics environment. *Computing in Science & Engineering*, 9(3):90–95, 2007.

[28] Jeff Reback; jbrockmendel; Wes McKinney; Joris Van den Bossche; Tom Augspurger; Phillip Cloud; Simon Hawkins; gfyoung; Sinhrks; Matthew Roeschke; Adam Klein; Terji Petersen; Jeff Tratner; Chang She; William Ayd; Patrick Hoefler; Shahar Naveh; Marc Garcia; Jeremy Schendel; Andy Hayden; Daniel Saxton; Marco Edward Gorelli; Richard Shadrach; Vytautas Jancauskas; Ali McMaster; Fangchen Li; Pietro Battiston; Skipper Seabold; attack68; Kaiqi Dong. *pandas-dev/pandas: Pandas*. Zenodo, July 2021.

[29] Jorge J. More Burton S. Garbow, Kenneth E. Hillstrom. Documentation for minpack subroutine hybrd. Technical report, Argonne National Laboratory, 1980.

[30] Richard H. Byrd, Mary E. Hribar, and Jorge Nocedal. An interior point algorithm for large-scale nonlinear programming. *SIAM Journal on Optimization*, 9(4):877–900, 1999.

[31] Luca Da Lio, Giovanni Manente, and Andrea Lazzaretto. A mean-line model to predict the design efficiency of radial inflow turbines in organic rankine cycle (orc) systems. *Applied Energy*, 205:187–209, 2017.

[32] Philip P. Walsh and Paul Fletcher. *Gas Turbine Performance*. Blackwell Science Ltd, 2 edition, 2004.

[33] Tolumoye John Ajoko. Design study for single stage high pressure turbine of gas turbine engines. *American Journal of Engineering Research (AJER)*, 03:296–305, 2014.

[34] Jet Engine Specification Database. Lyulka al-21f-3, military turbojet/turbofan specification. http://www.jetengine.net/miltfspec.html, 2005.

[35] Adrian Dahlquist. Investigation of losses prediction methods in 1d for axial gas turbines. Master's thesis, Lund University, 01 2008.

[36] S.L. Dixon. *Fluid Mechanics, Thermodynamics of Turbomachinery*. Pergamon International Library. Elsevier Science & Technology Books, 1978.

[37] Pamela Bugała. Review of design of high-pressure turbine. *Journal of KONES*, 24:67–76, 09 2017.

[38] Jorge Saavedra García. Gas generator for an automobile. Design Exercise, 2013-2014.

List of Figures

List of Tables